# UNIVERSITÁ DEGLI STUDI DI MILANO


## PhD Thesis in TRANSLATIONAL MEDICINE

XXXV CYCLE

# Spinal muscular atrophy organoids reveal developmental defects rescued by antisense oligonucleotides treatment

**PHD CANDIDATE:** IRENE FARAVELLI

**PHD SUPERVISOR**: CHIAR.MA PROF.SSA STEFANIA PAOLA CORTI

**PHD COORDINATOR:** CHIAR.MA PROF.SSA CHIARELLA SFORZA

ACCADEMIC YEAR 2021/2022

# INDEX

**ABSTRACT**

Spinal muscular atrophy (SMA) is a neuromuscular disease caused by mutations in the *SMN1* gene. Recent therapies have significantly modified SMA natural course, but treatment efficacy remains variable and the reasons beyond this variability are still largely unexplored. Identifying pre-symptomatic SMA features is crucial to define the optimal therapeutic window and most efficient strategy in order to increase drug efficacy. Recent studies have shown that patients start to develop pathological signs *in utero*, suggesting that SMA retains an important, and still under investigated, developmental phenotype.

In the present study, we generated SMA type 1 cerebral and spinal cord organoids (SCOs) to recapitulate human-specific early neurodevelopmental features. Single-cell transcriptomics revealed a pervasive transcriptional alteration in multiple cell populations, along with drastic changes in motor neuron gene expression. Morphological analyses detected early differentiation defects in SMA SCOs, unveiling a significant developmental component to the SMA pathology. Whole organoids electrophysiological acute recording revealed altered basal activity and pronounced hyperexcitability.

Optimized peptide-conjugated antisense oligonucleotide tested in SMA SCOs successfully reverted both morphological and functional deficits.

Of note, SMA cerebral organoids displayed similar functional deficits, revealing the widespread impact of the disease, beyond the spinal cord.

Our findings provide proof of concept that SMA organoids can be used for effective drug testing, while demonstrating early-onset and pervasive features of SMA, which need to be considered in the therapeutic perspectives.

**ABBREVIATIONS**

antisense oligonucleotides (ASOs); atlastin (ATL1); basic fibroblast grow factor (bFGF); bone morphogenic protein (BMP); bovine serum albumin (BSA); brain-derived neurotrophic factor (BDNF); cell-penetrating peptides (CPPs); central nervous system (CNS); differentially expressed genes (DEG); control (CTRL); doublecortin (DCX); embryoid bodies (EBs); fetal bovine serum (FBS); glial cell line-derived neurotrophic factor (GDNF); glutamate (glu); glycogen synthase kinase-3 (GSK3); heavy neurofilament (NF-H); high-density multielectrode array (HD-MEA); induced pluripotent stem cells (iPSCs); ingenuity pathway analysis (IPA); insulin-like growth factor-1 (IGF1); light neurofilament (NEFL); month (mo); morpholino (MO); motor neurons (MNs); neural induction media (NIM); neurexin (NRXN); paraformaldehyde (PFA); phosphate-buffered saline (PBS); precise time spike detection (PTSD); principal component analysis (PCA); quantitative real-time PCR (qRT-PCR); retinoic acid (RA); room temperature (RT); smoothened agonist (SAG); sonic hedgehog (SHH); spinal cord organoids (SCOs); spinal cord organoids differentiation media (SCODM); spinal muscular atrophy (SMA); stathmin2 (*STMN2*); survival motor neuron 1 (SMN1); survival motor neuron 2 (SMN2); synaptotagmin (*SYT*); transforming grow facotor β (TGF- β); tubulin (TUJ1); uniform manifold approximation and projection (UMAP); unique molecular identifiers (UMIs).

# INTRODUCTION

## ***Spinal Muscular Atrophy***

*Genetic Landscape*

Spinal Muscular Atrophy (SMA) was first described by Werdnig and Hoffmann back in the 19th century, when they independently reported clinical cases of young patients suffering from progressive muscular atrophy and paralysis [1]. Autopsy results revealed significant atrophy of the ventral roots and degenerations of motor neurons (MNs) in the anterior horn of the spinal cord as pathological hallmarks [2]. Decades of research led to the discovery that 95% of SMA cases are caused by mutations and/or deletions in the Survival Motor Neuron 1 (*SMN1*) gene. *SMN1* is located on chromosome 5q13[3]; humans also carry a paralogous gene (referred as *SMN2*) that differs from *SMN1* by a small pool of nucleotides, with the most significant difference being a C-T transition in exon 7. This modification creates a splicing alteration that leads to the skipping of exon 7 (SMNΔ7) in approximately 90% of *SMN2* transcripts, which are therefore unable to generate a full-length SMN protein[4]. Thus, only 10% of *SMN2* transcripts are translated into a functional protein, while the remaining transcripts generate a highly unstable protein that is rapidly degraded. Interestingly, the clinical phenotype correlates with the number of *SMN2* copies present in the genome [5,6]. Cases of asymptomatic carriers of homozygous *SMN1* mutations and multiple copies of *SMN2* have been reported, while the lack of *SMN* products is invariably fatal [7,8]. SMN complex genetic landscape has led to the creation of a*d hoc* preclinical models to investigate disease pathogenesis and test therapeutic compounds. This has been accomplished with the genetic insertion of two copies of *SMN2* and of a transgene expressing *SMN*Δ7 (lacking exon 7) in Smn-knockout murine embryonic cells (Smn−/−; SMN2/SMN2; SMNΔ7/SMNΔ7)[9]. SMNΔ7 mice display an early neuromuscular phenotype with an average lifespan of about 2 weeks and are one of the most common mouse model employed for SMA preclinical research [4,10–13].

*Pathogenesis*

The functional product of *SMN1* and *SMN2* is the full-length ubiquitously expressed SMN protein; high SMN levels can be found in the brain, spinal cord, kidney and liver [14]. Complete lack of SMN in model organisms is lethal as it likely is in humans, where the absence of both *SMN1* and *SMN2* has never been reported. In contrast, ubiquitous SMN reduction, such as the one displayed by severe SMA patients, appears to be differentially tolerated by each tissue, with the nervous system particularly affected[15].

SMN holds several domains that are fundamental for its interaction with other proteins to build the SMN complex, a multimeric structure essential for the assembly of small nuclear ribonucleoprotein (snRNPs). snRNPs tightly regulate pre-mRNA splicing and histone pre-mRNA 3'-end processing [16,17]. Thus, SMN is upstream a cascade of molecular processes playing a key role in RNA splicing. In addition, SMN has been implicated in the formation of several other cellular snRNPs involved in axonal mRNA trafficking and translation[18].

Thus far, the genetic and phenotypic hallmarks of SMA have been recapitulated in different mouse models, which have proven to be a powerful platform for investigating disease pathological mechanisms[19]. Through similar approaches, the first SMA mouse models were engineered to express reduced levels of SMN by harboring two copies of the human *SMN2* transgene with concomitant knockout of the single mouse Smn gene[20,21]. These SMA mice display a normal phenotype at birth, while after some days they start to develop a severe motor impairment, muscle atrophy and reduced weight gain; survival is dramatically decreased (approximately one week of age after birth). Further studies led to the addition of the SMNΔ7 cDNA transgene to this genetic background; this strategy increased the median survival to approximately two weeks of age, providing for the most widely employed SMA models to date[4].

Cellular pathology showed degeneration of MNs in the spinal cord with segment-specific vulnerability along the rostro-caudal axis[4,20,22]. Additional alterations have been reported at the synaptic levels, with reduced inputs on MN soma. Disruptions within these neural networks play an important role in the SMA phenotype, as SMA MNs receive decreased glutamatergic synaptic inputs from the proprioceptive sensory neurons and local spinal interneurons. SMA mice showed a significant impairment of the sensory-motor neurotransmission associated with the dysfunction of the proprioceptive synapses. In parallel, electrophysiological analyses revealed that SMA MNs exhibit elevated intrinsic excitability and altered firing properties[22,23].

Neuromuscular junctions (NMJs) were also significantly altered by the disease; morphological studies showed presynaptic neurofilament accumulation, reduced vesicle content, aberrant postsynaptic acetylcholine receptor clustering and motor endplate development[24–26]. Furthermore, reduction of SMN in Schwann cells appeared to cause alterations in the myelination pattern of peripheral nerves [27].

In sum, SMA has emerged as a disease characterized by the concurrent dysfunction of multiple components of the motor system and not only degeneration of MNs.

Defects in heart, pancreas, and liver have been documented in severe SMA preclinical models and patients [10,28–30]. Defects in cognitive function, brain neuropathology and imaging have also been reported in SMA patients, but only partially documented[31]. The early events that drive degeneration and their impact on the entire central nervous system (CNS) are still largely unknown and key to modeling the disease. The systemic SMA phenotype highlighted by recent studies poses an important challenge to the treatment of this disease. SMN restoration might be essential for multiple cellular compartments, and cell populations, not only located in the CNS, to reach fully significant therapeutic outcomes.

*Developmental Features*

Even though SMA is a genetic condition, very little material is available from the prenatal stages of the human disease. Published data derives from studies on foetuses diagnosed through prenatal genetic testing requested for positive family history[32,33]. SMN protein is highly expressed in foetal CNS[34]; postnatally, its levels decrease markedly in most tissues, suggesting that SMN is particularly needed during the first stages of the development. Neuropathological analyses carried out on SMA foetal spinal cords have reported that the total MN number is diminished in comparison with age-matched controls starting from the 12th week of gestation and throughout the entire prenatal life[33].

These data suggest that the physiological process of programmed apoptosis that normally occurs during development is increased in SMA individuals leading to an early loss of MNs. Of note, recent reports have described that SMA MNs display a reduced number of synaptic contacts on their soma; some of these results also imply that this process occurs before degeneration suggesting that synaptic deafferentation may precede MN death[22,23,35,36].
Importantly, axonal growth, maturation and also myelination appear to be affected. Recent data from human SMA autopsies showed that abnormal MN axon development *in utero* is associated with very rapid post-natal degeneration in SMA[37]. The percentage of MN reduction and the entity of their dysfunction in the developmental stage directly conditioned the age of disease onset and its severity[37].

Overall, these findings suggest that SMN reduction impacts early neural development processes, affecting multiple compartments of the motor unit. The specific molecular events leading to degeneration and their role in the entire CNS (and extra CNS) network is still matter of investigation.

A recent work published by Motyl at al.[38] reported the evidence of pathological features during early embryonic development in a mouse model of severe SMA. At embryonic day 14.5, SMA embryos were overall smaller with decreased heart size. Interestingly, these alterations preceded symptomatic motor impairment by about two weeks. Moreover, they were associated with widespread perturbations in the proteomic profile of the brain, spinal cord, skeletal muscles, and liver of SMA embryos in comparison with healthy controls.

At closer observation, the extent of overlap between the proteomic alterations in the affected tissues was very low, and the degree of SMA proteome deregulation in each tissue did not seem to correlate with the SMN protein levels.

These results further point to a tissue-specific effect of SMN reduction early in development, with a significant clinical impact on the treatment regimen.

*Clinical Phenotype*

SMA prevalence ranges from 8 to 10 per 100,000 individuals with an incidence of 1:10,000 live births [39,40]. Affected individuals suffer from different degrees of muscular wasting mainly involving proximal muscles and usually starting from the lower limbs. SMA has been classified into 4 main clinical forms along a decreasing spectrum of severity, taking into account the age of onset, the reached motor milestones and the average life expectancy [41].

SMA type 0 (prenatal onset SMA) is the most severe subtype with an onset during *in utero* development with reduced fetal movements. At birth, patients are not capable to swallow and present facial diplegia and joint contractures. Life expectancy is usually reduced to the first weeks after birth [42].

SMA type 1 (Werdnig-Hoffman disease) accounts for 50% of all cases and is the most common clinical form. Patients usually present a homozygous *SMN1* deletion in the presence of two copies of the *SMN2* gene and start developing symptoms during the first months of life ($5^{th}$-$6^{th}$ month). Without specific treatments, life expectancy is reduced to the second year of life [43]. Affected children never reach basic motor milestones and they are not able to sit autonomously. Patients suffer from generalized muscular wasting with significant hypotonia (floppy infant syndrome with frog-leg position due to proximal muscles hypotonia). Deep tendon reflexes are very reduced or absent. Impairment in ribcage expansion can lead to bell-shaped thorax. Affected children experience trouble in breathing and feeding along with tongue fasciculations and poor cry, as consequences of the involvement of bulbar MNs.

Systemic involvement may include congenital heart defects with potential impairment of the cardiac autonomic innervation, gastroesophageal reflux, constipation and metabolic dysfunction with weight loss [29,44,45].

SMA type 2 (Dubowitz disease) onset ranges from 7 to 18 months after birth. Affected children reach the ability to sit when properly positioned, and in some cases are able to stand even though they do not walk [46]. SMA type 2 patients have in general reduced life expectancy, with a range from 2 to over 40 years.

SMA type 3 (Kugelberg–Welander disease) is highly heterogenous in the clinical phenotype. Patients usually retain the ability to sit, stand and ambulate at least until puberty, when many individuals cannot ambulate anymore [47]. SMA type 3 patients suffer from different degrees of muscular hypotonia with a preferential wasting of proximal muscles. Bulbar MNs are less frequently affected. The clinical natural history is quite stable with a life expectancy often similar to the general population [46].

SMA type 4 has an onset during adulthood (after the second or third decade of life) and represents the mildest form. Patients remain able to walk, even though they can variably display signs of spinal MN degeneration, such as muscular hypotonia and atrophy, fasciculations and reduced deep tendon reflexes. The disease course is generally stable and affected individuals have a life expectancy comparable to the general population [48].

To summarize, SMA is a comprehensive term for a wide spectrum of clinical conditions primarily united by the significant loss of spinal MNs, associated to a complex variety of accompanying signs and symptoms pointing towards an early and pervasive role of SMN.

*Diagnostic and Therapeutics*

Molecular genetic analysis represents the gold standard diagnostic test for SMA [49,50]. Due to its high frequency, SMA should be considered in every presenting case of floppy infant.

In more than 95% of all cases, SMA is caused by either a homozygous *SMN1* deletion in exons 7-8 or a gene conversion involving *SMN1* and *SMN2* genes [51,52]. In the remaining cases, the pattern of inheritance is represented by a compound heterozygosis with a single *SMN1* deletion and a different mutation in the other copy of the gene [53]. Thus, the first diagnostic strategy points towards unveiling homozygous *SMN1* deletions, while second-level approaches include *SMN1* dosing and sequencing to investigate compound heterozygosis. The specificity of the test is nearly 100% and the sensitivity of 95% [43].

Carrier testing and prenatal screening have become increasingly available. It needs to be considered, however, that the prenatal testing is not always able to fully predict the severity of the clinical outcome, since the number of copies of *SMN2* can vary for each SMA subtype (i.e. two copies of *SMN2* could result in either SMA type 1 or type 2 phenotype) [6].

Universal newborn screening programs for SMA are being implement worldwide and this will help in dampening the variabilities that are still present in diagnosis and management, also allowing to better evaluate which patients could benefit of specific treatments[54,55]. In this context, the development of biomarkers predictive of treatment response along with a consensus on the outcome measures would improve clinical trial enrollment and therapeutic efficacy assessment [52,56].

Recently, breakthrough therapeutic strategies developed to restore the levels of SMN have received FDA/EMA approval and are currently in clinical use[57,58]. These approaches are based on either cDNA replacement of *SMN1* or the use of antisense oligonucleotides (ASOs) or small molecules to achieve splicing correction of *SMN2* [59].

Nusinersen has been the first ASO marketed as disease-modifying drug for SMA. It is administered intrathecally by lumbar puncture and binds to an intronic splice-silencing-site in intron 7 of *SMN2* inhibiting the action of other splice-factors and leading to the translation of a fully functional SMN protein.

These drugs have dramatically changed the clinical prognosis of all four SMA types, and for the fatal to severe SMA type 1, are able to reduce the disease to a chronic condition by halting or preventing motor disability. However, the greatest impact is achieved when patients are treated pre-symptomatically. Although growing clinical data show that approved treatments also provide benefits in the chronic phase, an unmet therapeutic need remains for patients treated after symptom onset[57] and our understanding of the factors halting the treatment efficacy is elusive.

In addition, observed variability in treatment response, and the impact on tissues other than the spinal cord still need to be addressed. Therefore, a better understanding of SMA disease mechanisms in the early disease stages, even prenatally, is pivotal to optimize current therapeutic approaches by increasing efficiency and targeting/biodistribution and to develop new therapeutic strategies.

***Neural organoid biology***

Model organisms can only partially recapitulate the complex features of the human CNS. Specific human neural progenitors, such as outer radial glia, are not represented in the mouse brain and even though murine models have provided precious insights into neurodevelopment, the high complexity of the human CNS cannot be fully reproduced in animal models. Moreover, the inaccessibility of the human brain during *in utero* development has hampered progresses in disease modelling and therapeutic findings.

The discovery of novel human 3D *in vitro* models has represented a major achievement in the field of disease modelling. Human pluripotent stem cells can be obtained from skin fibroblasts or peripheral blood cells, which can be reprogrammed into induced pluripotent stem cells (iPSCs) with the use of specific factors [60]. IPSCs can be then cultured in suspension with selected media and inducing molecules to generate organoids, which are a 3D assembly of cells with the capability of self-assembly in distinct regions, recapitulating *in vitro* the main features and functions of a specific organ.

Different protocols have been developed to generate cerebral organoids able to recapitulate the endogenous neurodevelopmental program, providing the complex landscape of most brain cellular subtypes[61,62]. Lancaster and colleagues pioneered the field with the production of cerebral organoids generated through the formation of embryoid bodies included in Matrigel droplets to provide an efficient scaffold for growth[63]. These organoids include different cerebral cellular populations, and they show a rough organization in superficial (SATB2+) and deep (CTIP2+) layers, although in absence of any structural II-VI layers organization.

In the last years, multiple groups have worked on developing organoids of different neural structures, such as the retina[64], the hippocampus[65], and finally the spinal cord[66].

Andersen and colleagues developed an interesting model based on the assembly of cortical spheroids (induced with the use of patterning factors) spinal cord spheroids (generated with the use of caudalizing and ventralizing small molecules) and muscular spheroids[66]. In this way, they not only achieved a high level of tissue complexity recapitulating most spinal cord cellular populations, but they were also able to unveil connectivity among the different tissues. When the cortical spheroid was externally stimulated, the impulse could be carried along the assembloid and resulted in contractions of the muscular spheroid.

The achievement of complex *in vitro* models has been paralleled by great advances in sequencing techniques and computational analyses. Nowadays, it is indeed possible to molecularly deconvolute the cellular composition of a given tissue allowing to determine single cell perturbations. In this context, we might start to elucidate the mechanisms triggering neuronal susceptibility to degeneration, a phenomenon that is crucial for pathogenetic studies and therapy discoveries.

# AIMS OF THE STUDY

The underlying hypothesis of this project is that early neurodevelopmental alterations are present and pervasive in SMA and contribute to terminal degeneration**.**

In this context, human neural organoids are a fitting neurodevelopmental model to investigate specific human developmental process and investigate the cellular and functional mechanisms leading to SMA disease signatures.

Organoid models have been extensively employed to investigate human disorders such as neuropsychiatric and neurodegenerative conditions [63,67–69]; in this context, spinal cord organoids represent a precious tool for studying SMA and other conditions characterized by MN degeneration.

Moreover, recent clinical and preclinical studies have shed light on a potential involvement of cortical neurons in SMA pathology[19,32,70,71]. Thus, the reduction of SMN could cause a pervasive CNS network perturbation contributing to the early degeneration of the more vulnerable spinal MNs.

The present project will be articulated through the following aims:

- Generation of an efficient protocol for the generation of (iPSC)-derived spinal cord organoids (SCOs).
- Characterization of derived SCOs with morphological and functional approaches in order to demonstrate that they can be successfully used to elucidate early clinically relevant SMA pathological phenotypes.
- Molecular dissection with the use of single-cell RNA sequencing to investigate SMA- and MN-specific molecular changes in transcripts involved in cell differentiation, survival, and neuronal function.

- Treatment of SMA SCOs with a peptide-conjugated ASO with morpholino chemistry targeting SMN levels.
- Assessment of compensation of morphological and functional alterations in SCOs by the treatment; this can provide proof of concept that SMA organoids are a powerful tool for drug testing and target optimization with a significantly impact on the current therapeutic strategies.
- Generation of CTRL and SMA brain organoids following a previously published differentiation strategy[61]. The goal is to study alterations in basal and evoked electrophysiological activity beyond the spinal cord involvement, supporting the presence of early functional impairment in the CNS, only hypothesized thus far and not experimentally assessed.

# Results

## Spinal cord organoids reveal complex cellular composition

We derived human SCOs from healthy control and SMA type 1 patients iPSC lines (**Fig. 1-3,** n=3 lines each) using a free-floating 3D culture method. Spinal cord development is a complex process that entails both rostro-caudal specification mediated by Wnt and retinoic acid (RA), and dorso-ventral patterning downstream of sonic hedgehog (SHH) signaling [72,73].

Thus, SCOs were cultured in the presence of small molecules known to recapitulate the *in vivo* signaling specification[74–76] (**Fig. 1**).

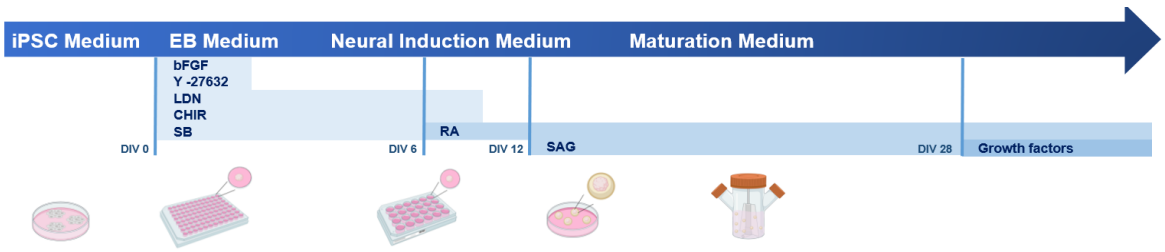


**Figure 1. Spinal cord organoid generation;** schematic representation of the differentiation protocol

In both CTRL and SMA organoids, the treatment promoted a progressive caudal neuralization with the appearance at the early differentiation stage (1 month) of progenitor markers (OLIG2, **Fig. 2c-d and 3c**), followed by the appearance of the neuronal markers DCX and SMI32 (**Fig. 2d and 3c**). As the differentiation proceeded, we observed the presence of spinal precursors expressing HOXB4, and ISL1 positive MNs (**Fig 2d and 3c**). At 2 months, we also detected the presence of astroglial cells positive for GFAP (**Fig 2d and 3c**). Together, the data show that SCOs can recapitulate key aspects of spinal cord neurogenesis.

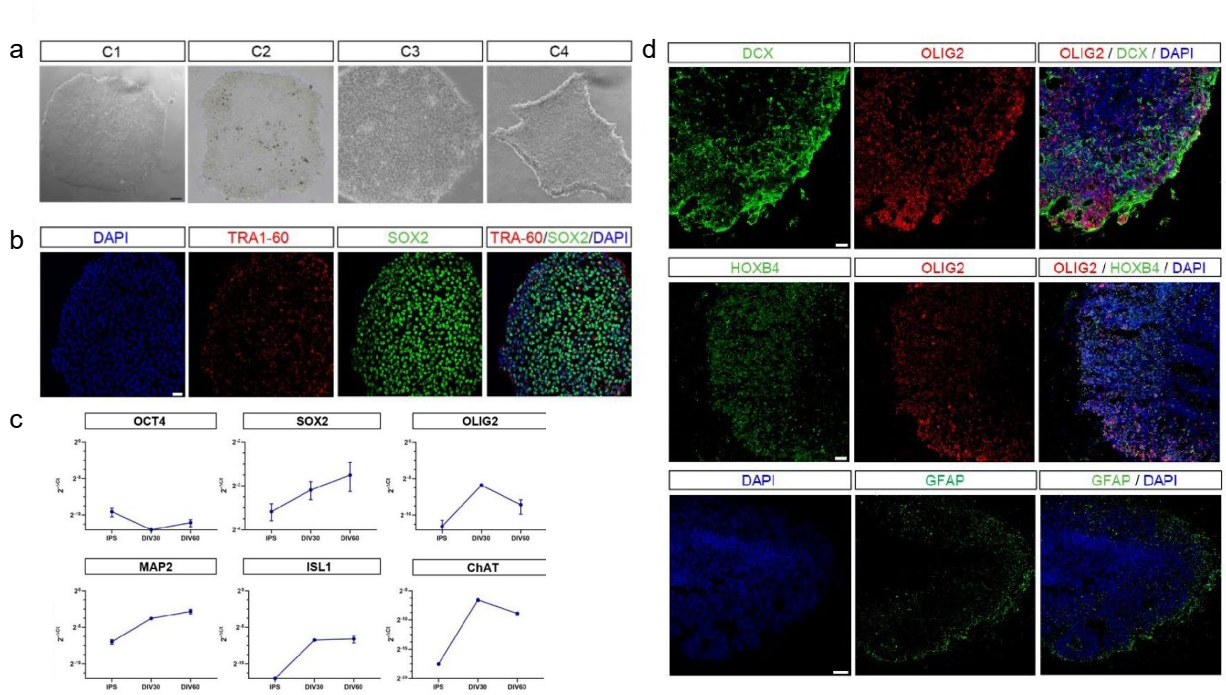


**Figure 2**. **CTRL Spinal cord organoid characterization.** (**a**) Brightfield images of differentiation pathway progression. Scale bar: 50 µm. **b**, Stem cell marker staining in iPSCs. Scale bar: 50 µm. **c**, qPCR analysis of CTRL SCOs showed expression of neural and spinal genes over time. $n \geq 3$ SCOs from one line; data are represented as mean ± SD. **d**, Different neural (OLIG2, HOXB4 and DCX) and glial (GFAP) subpopulations were identified by immunofluorescence within the organoids. Scale bar: 50 µm. Nuclei were stained with DAPI (blue).

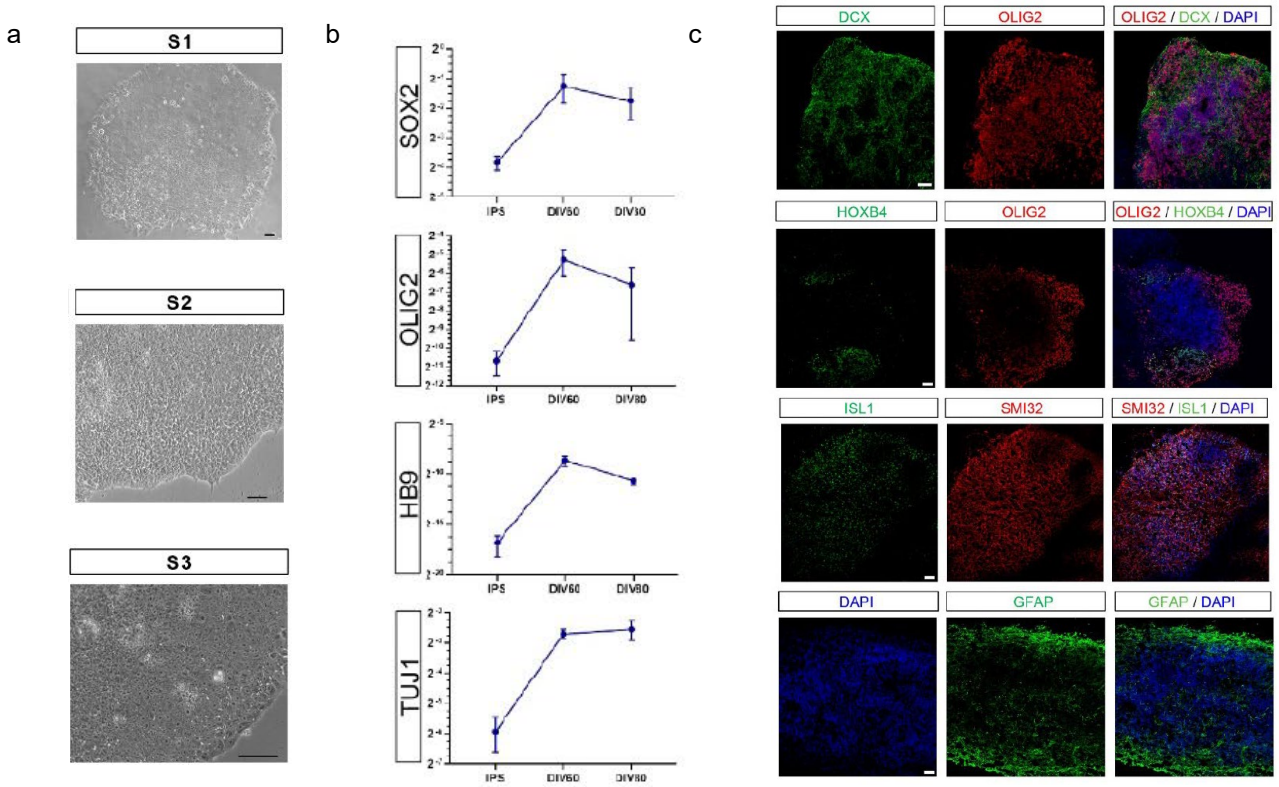


**Figure 3. SMA Spinal cord organoid characterization. a**, Representative bright-field images of SMA iPSCs. Scale bar: 50 µm. **b**, qPCR analysis of SMA SCOs showed expression of neural and spinal genes over time. $n$=3 SCOs from two lines; data are represented as mean ± SD. **e**, Different neural and glial (GFAP) subpopulations were identified in SMA SCOs. Scale bar: 50 µm. Nuclei were stained with DAPI (blue).

## SMA spinal cord organoids display molecular disease signatures

To address the early phases of SMA organoids development, we analyzed 2-month-old CTRL and SMA SCOs composition by single-cell RNA-sequencing (**Fig 4a-b**). We sequenced single cells from two different SCOs deriving from both CTRL and SMA lines and successfully profiled 14,941 cells from SCOs across all the lines. Unsupervised graph-based clustering identified nineteen clusters (**Fig 4a**).

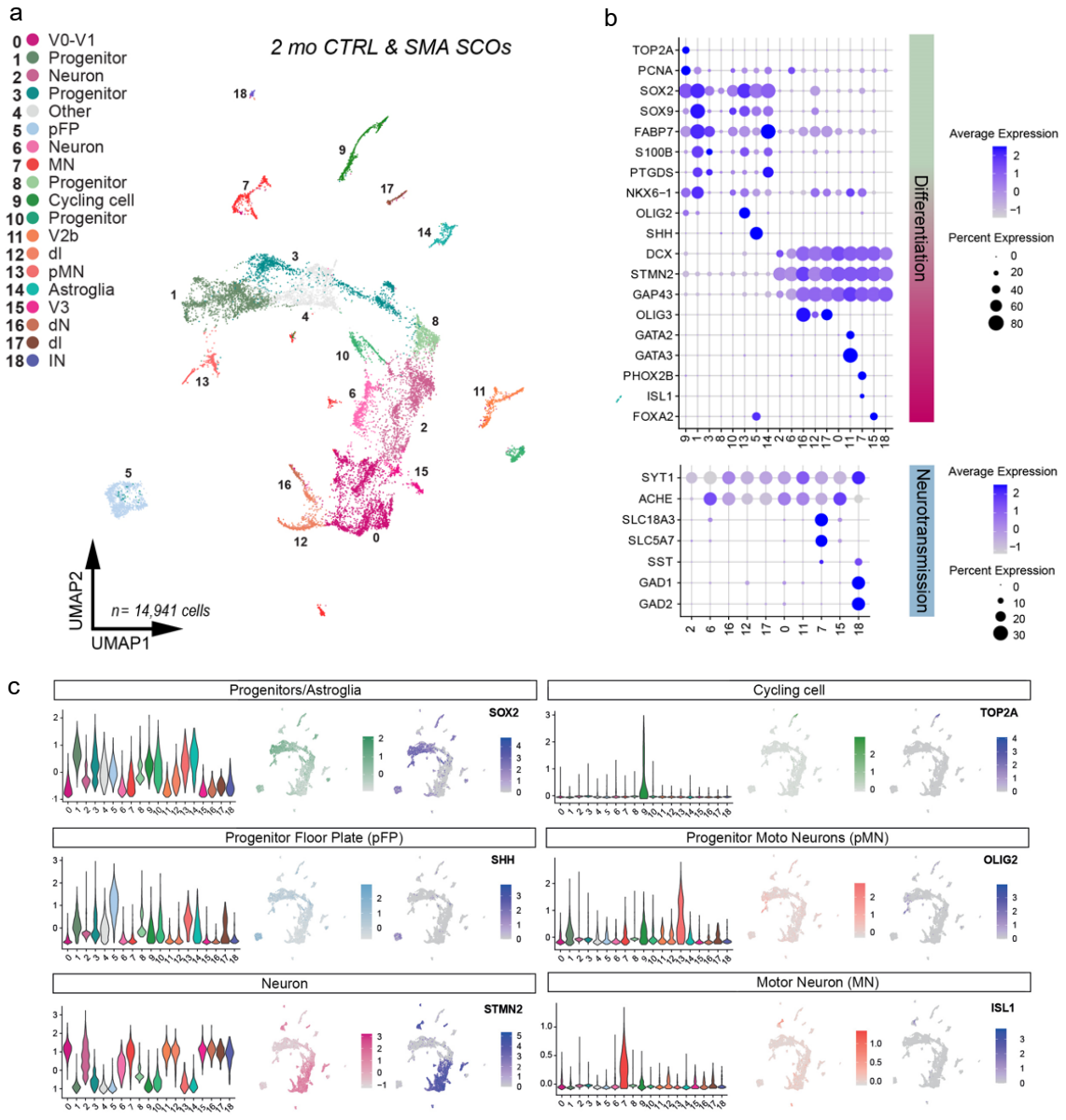


**Figure 4. Molecular landscape of spinal cord organoids. a**, CTRL and SMA single cell RNA-seq at 2 months (mo). Unsupervised UMAP subdivides SCOs into cycling cell (c9), neural progenitors (c1, c3, c8, c10, P), floor plate progenitors (c5, pFP), motor neuron progenitors (c13, pMN) differentiating neuronal cells (c2, c6, N), and several subtypes of ventral neurons (c0, c7, c11, c15), dorsal neurons (c16, dN), interneurons (c12, c17, c18) and

astroglia (c14). **b**, Dot plots showing cluster-specific expression of representative genes associated with cell differentiation and neurotransmission; dot size corresponds to the percentage of cells in a cluster expressing each gene and the color corresponds to the average expression level (from gray to violet, low to high). **c**, Violin plots showing module score enrichment in individual clusters for selected relevant cell populations.

Module annotation with defined sets of genes for dorsal and ventral genes identified proliferative cells (cycling, cy, characterized by the expression of *TOP2A, MKI67*), neural progenitors (P, *SOX2, SOX9*), differentiating neurons (N, *DCX*), and several subtypes of spinal cord neurons such as interneurons (dI, IN, *GAD1*, *GAD2*) and neurons of dorsal (dN, *OLIG3*) and ventral (v0-v1, v2b, v3, *GATA2, GATA3, FOXA2,* respectively) domains (**Fig.4c**). At this stage, we could also identify distinct clusters of MN precursors (pMN, *OLIG2*) and postmitotic MNs (MN, *ISL1, PHOX2B*) (**Fig. 4c**).

Overall, these results confirm that SCOs represent robust tools for modeling neurological diseases with multicellular involvement, such as SMA.

To begin analyzing SMA alterations in SCO models, we performed differential gene expression analysis in each cluster (absolute log fold change ≥ 0.2, min.pct = 0.25 and adjusted *p*-value < 0.05) and found an overall transcriptional alteration in multiple precursor types and neuronal classes in SMA in comparison with CTRL SCOs (**Fig. 5a**).

In accordance with the renowned susceptibility of spinal MNs in SMA pathogenesis, the largest proportion of deregulated genes (1061 genes differentially expressed between CTRL and SMA SCOs, 479 upregulated and 582 downregulated) was observed in cells ascribed to the MN cluster (**cluster 7, Fig. 5b**). In particular, SMA MNs showed downregulation of genes involved in neuronal growth and synaptic maturation, including genes previously described as targets of the SMN complex[76].

In line with previous results in 2D cultures and animal models that have reported reduced length and branching alterations in SMA MN axons[77,78], we also found axon-related molecules (*NEFL*, *ATL1*) and synaptic proteins, as stathmin2 (*STMN2*)[79,80], synaptotagmin (*SYT4, SYT5, SYT7, SYT17*) and neurexin (*NRXN1* and *NRXN2)*[76,81] significantly deregulated in the MN clusters (**Fig. 5b-c**).

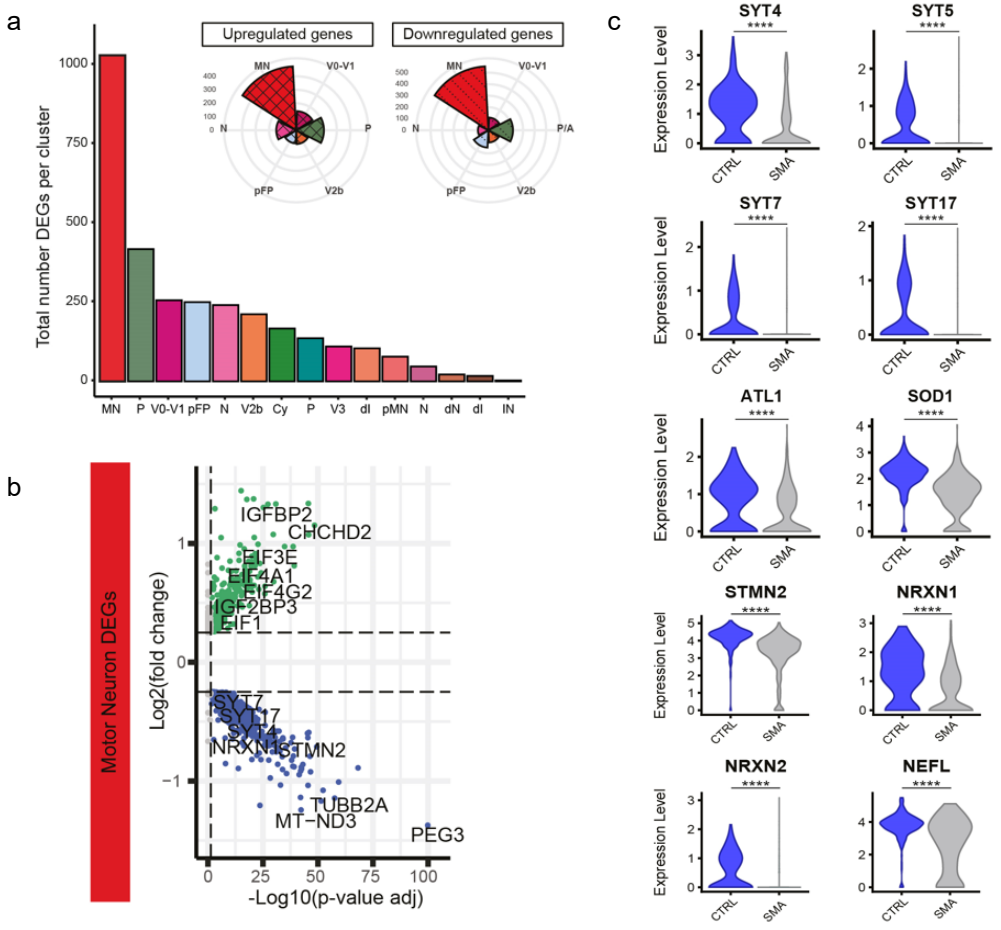


**Figure 5. SMA molecular disease features. a**, Numbers of deregulated genes across different clusters and rose plots showing the numbers of upregulated and downregulated genes for the six most strongly affected clusters. **b**, Volcano plot of differential gene expression in the MN cluster in SMA SCOs relative to CTRL. Values of log2 fold change are plotted against −log10 of the adjusted *p*-value for each gene. Green denotes genes upregulated in SMA while blue denotes genes downregulated in SMA (absolute log fold change ≥ 0.2, min.pct = 0.25 and adjusted *p*-value < 0.05, thresholds plotted as dashed lines). Non-significant genes are shown in grey. **c**, Violin plots of synaptic and disease related genes deregulated in the MN cluster from SMA SCOs in comparison with CTRL SCOs (SYT4 adjusted *p*-value = $1.289 \times 10^{-16}$, SYT5 adjusted *p*-value = $3.793 \times 10^{-10}$, SYT7 adjusted *p*-value = $2.652 \times e^{-07}$, SYT17 adjusted *p*-value = $4.760 \times e^{-12}$, ATL1 adjusted *p*-value = 0.00037, SOD1 adjusted *p*-value = $7.765 \times e^{-35}$, *STMN2*, adjusted p-value = $1.721 \times e^{-34}$; *NRXN1*, adjusted p-value = $2.049 \times e^{-12}$; *NRXN2*, adjusted p-value $5.677 \times e^{-11}$; *NEFL*, adjusted p-value = $4.343 \times e^{-14}$; non-parametric Wilcoxon rank sum tests).

Previous results in 2D cultures and animal models have reported alterations in SMA axons that display reduced length and branching[77,78]. To investigate this feature in our 3D model, CTRL and SMA organoids were mechanically dissociated, and approximately 50,000 cells were plaited and maintained in culture. A significant reduction in axonal length, measured with staining for the post-mitotic marker SMI32, was observed in SMA neurons derived from dissociated SCOs (CTRL 58.34 ± 11.76 µm *vs*. SMA 33.53 ± 8.46 µm, $p < 0.0001$; **Fig. 6a-b**). This result nicely correlates with recent data on human SMA autopsies finding abnormal MN axon development *in utero*[37], which was associated with very rapid post-natal degeneration.

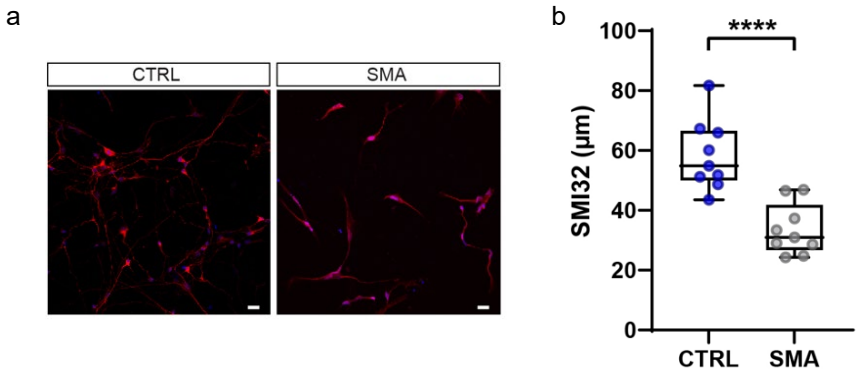


**Figure 6. Axonal length in CTRL and SMA dissociated organoids. a**, Representative image of dissociated SMA organoids that display reduced SMI32-stained axon length in culture. Scale bar: 20 µm. **b**, Quantification of (**a**). Axon length is significantly lower in SMA than CTRL SCOs (unpaired *t*-test, $p < 0.0001$, $n = 9$ SCOs from two CTRL and three SMA lines)

Leveraging the cellular complexity of the SCO model, we observed altered gene expression in several cellular clusters (**Fig. 5a**) beyond MNs in SMA SCOs. We therefore sought to investigate the degree of overlap of molecular pathways implicated in SMA-specific alterations shared among different neuronal subtypes and progenitors.

By performing an integrated pathway analysis (using Reactome database), we found that mitochondrial respiration and cellular metabolism were significantly enriched in all the subpopulations analyzed, suggesting that defects in these cellular events might impinge on virtually all SCO SMA cells. Pathways related to splicing activity were mainly affected in neurons, while terms related to neuronal development and axonogenesis, as well as cellular

death (both apoptosis and autophagy) showed specific enrichment for the SMA MN cluster (**Fig. 7)**. This confirms that MNs are indeed the most vulnerable neuronal subtype in SMA organoids but supports the idea that other types of neurons and progenitors also present specific alterations, thus pointing to a more pervasive scenario than previously anticipated, especially at early stages of development.

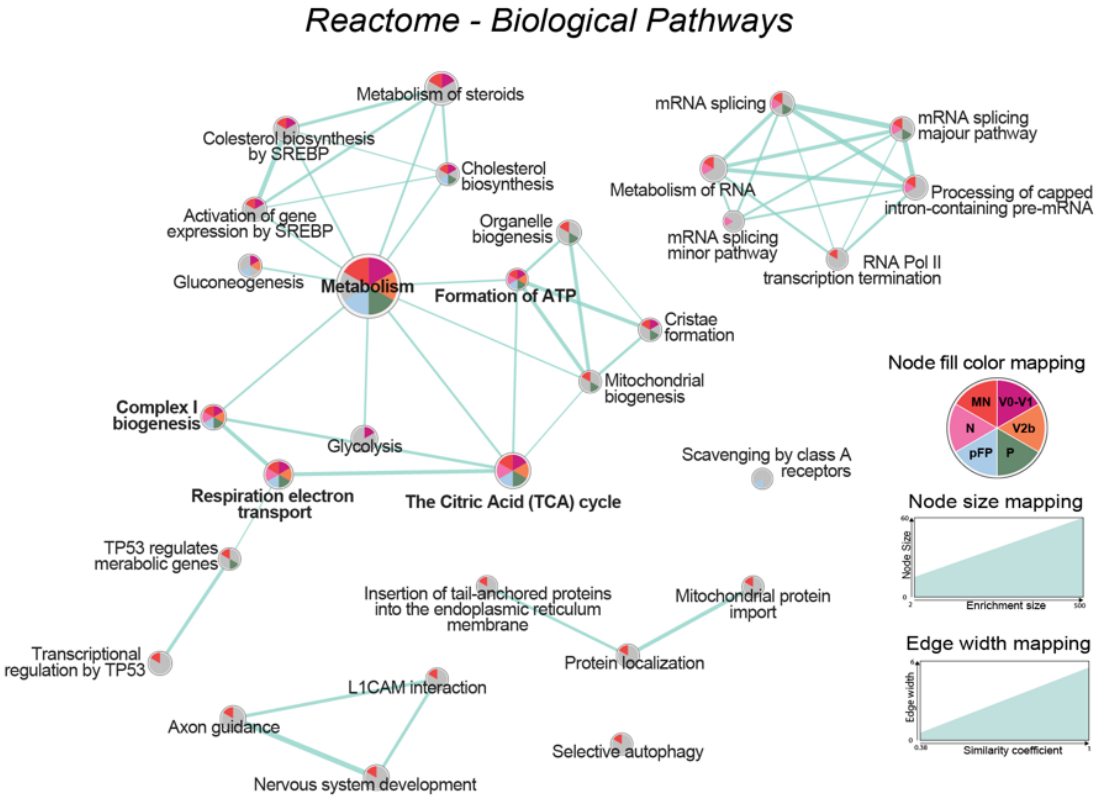


**Figure 7**. **Pathway analysis in spinal cord organoids.** Reactome analysis of CTRL and SMA SCOs of differentially regulated genes in the most strongly affected cell clusters (V0-V1 – cluster 0; Progenitor – cluster 1; Progenitor Floor Plate – cluster 5; neuron – cluster 6; MN – cluster 7; V2b – cluster 11) identified deregulated pathways including apoptosis and neuronal development. Node size and edge width parameters are represented in the legend.

Overall, SMA SCOs show a consistent molecular signature of disease across populations, accompanied by a distinctive deregulation of genes specifically associated with MN development and survival, as well as synaptic function and axonal stability.

## SMA organoids present alterations in neuronal differentiation

Since the transcriptional profiling suggested alterations in both SMA progenitor and neuronal types, we sought to determine whether SMA SCOs displayed changes in differentiation dynamics at the cellular level. We performed high-content image analysis assessing SCO neuronal morphology (**Fig. 8a-b**). Expression of the post-mitotic neuronal marker TUJ1 was severely decreased at 2 months in SMA SCOs, in accordance with the defect in differentiation and maturation in SMA SCOs observed (CTRL 33.21% ± 12.78 vs SMA 13.54% ± 8.648, p = 0.0005). Previous studies reported that neuropathological analyses of SMA human fetal spinal cords showed a decrease in the total MN number starting from gestational week 12 throughout the prenatal life in comparison with age-matched controls[33]. SCOs recapitulate the very early stage of spinal cord development, and our data suggest that the physiological process of cell death could be enhanced early in SMA. Using the TUNEL assay, we found that SMA SCOs exhibited a marked increase in apoptosis over time in comparison with CTRL SCOs (percentage of apoptotic nuclei in each organoid at 1 *vs*. 2 months: CTRL 11.3% ± 2.512 *vs.* 10.52% ± 4.369, $p = 0.8304$; SMA, 4.245% ± 2.372 *vs.* 17.6% ± 7.047, $p<0.0001$; **Fig. 8c-d**).

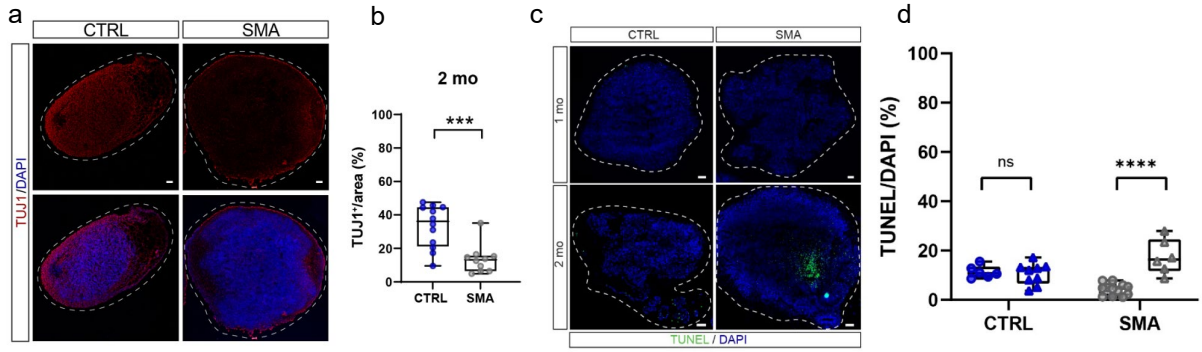


**Figure 8. SMA neurodegenerative features. a**, Representative images of TUJ1 (red) staining of CTRL and SMA SCOs at 2 mo. Scale bar: 100 µm. Nuclei were stained with DAPI (blue). **b,** Quantification of TUJ1 at 2 mo as intensity/area. CTRL SCOs show greater TUJ1 expression than SMA SCOs ($p = 0.0005$, unpaired *t*-test; $n \geq 10$ organoids from three CTRL and two SMA lines). **c**, Representative images of TUNEL (green) staining of CTRL and SMA SCOs at 1 and 2 mo. Scale bar: 200 µm. Nuclei were stained with DAPI (blue). **d**, Quantification of TUNEL-positive cells (as a percentage of cells revealed by DAPI staining) at 1 (circles) and 2 mo (triangles). $n \geq 6$ organoids from two CTRL and three SMA lines. Two-way ANOVA, Sidak's multiple comparisons test: $p = 0.8304$ and $p < 0.0001$ for CTRL and SMA, respectively. The proportion of TUNEL-positive cells increased significantly at 2 mo in comparison with 1 mo in SMA but not CTRL SCOs.

## SMA SCOs specific cellular features are rescued by SMN increase

Among the approved therapies for SMA[59], nusinersen is based on an antisense oligonucleotide (ASO) acting on *SMN2* (ASO_10-27), increasing the overall levels of SMN protein.

A 25nt MO oligo sequence against the ISS-N1 region of SMN2 (HSMN2Ex7D(-10-34)) was designed in our lab and combined local and systemic administration of MO in transgenic SMA mice effectively increased SMN full-length expression leading to robust neuromuscular improvement and survival rescue [82]. In a head-to-head comparison, MO-10-34 appeared more effective than previously described sequences (for reference, see [83]). However, important challenges of ASO-mediated therapy for SMA patients include improving the efficiency of the delivery, in particular in the CNS, ameliorating transport across the blood brain barrier, and extending the therapeutic window. MO treatment is apparently effective only in a pre-symptomatic phase and this could be due to an impaired uptake of MO by cells and tissues, when it is administered at a later stage of the disease. Cell-penetrating peptides (CPPs) are small cationic peptides (~10 to 30 amino acids) that have been demonstrated to be efficacious in transmembrane delivery of macromolecule compounds, such as oligonucleotides [84,85]. CPPs can be readily conjugated to charge-neutral MOs. This method has improved systemic delivery of MOs and ASOs in many disease models, like Duchenne muscular dystrophy [86,87].

To evaluate whether SMA SCOs could provide a useful system in which to test the efficacy of therapeutic molecules and whether specific disease features could be corrected by increasing SMN levels, we tested a recently validated ASO for *SMN2* with an optimized morpholino chemistry (MO-10-34$^{r}$[88,89]) conjugated with an arginine-rich cell-penetrating peptide (r6-MO). We recently demonstrated that the novel r6 can increase drug biodistribution and efficacy in animal models[83].

A significant increase in SMN expression was observed in protein lysates from organoids treated with r6-MO compared to untreated organoids ($p$ = 0.001; **Fig. 9a-b**).

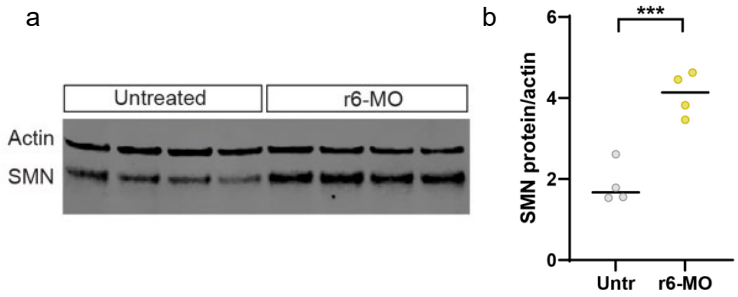


**Figure 9. MO treatment rescues SMN protein levels in SMA organoids. a,** Western blot analysis for SMN protein of untreated and r6-MO–treated SMA SCOs at 2 mo. b, Quantification of (**a**), $n$ = 4 for each group. Statistical analysis was performed using unpaired t-test; p = 0.001.

Notably, the differentiation phenotype was completely restored by MO treatment (percentage of cells positive for TUJ1: SMA 17.49% ± 5.468, *vs* r6-MO 33.05% ± 8.386, $p$ = 0.0014) (**Fig. 10a-b**). The administration of r6-MO at day 45 was able to significantly prevent cell death (percentage of apoptotic nuclei in each organoid at 2 months: untreated 18.27%±4.097 *vs.* r6-MO 10.54%±2.629, $p$ = 0.0192; **Fig. 10c-d**), supporting the idea that early intervention could halt the aberrant cellular processes, positively changing the course of the disease.

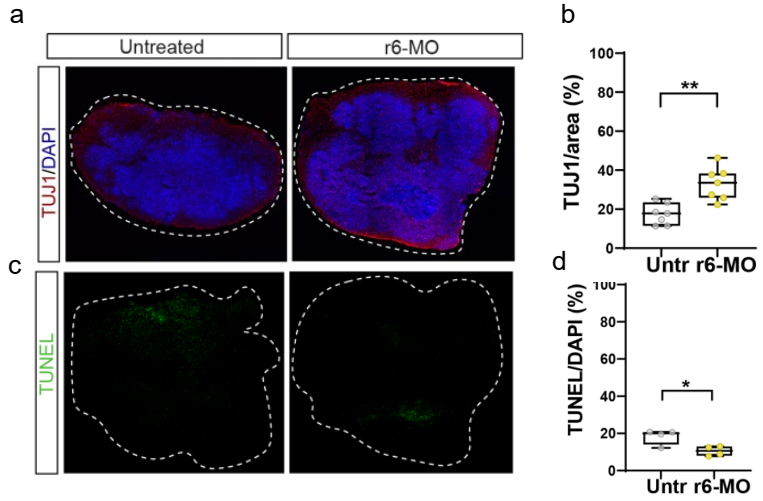


**Figure 10. SMA morphological alterations are rescued by the treatment**. **a**, Representative images of TUJ1 (red) staining of Untr and r6-MO SCOs at 2 mo. Scale bar: 300 µm. Nuclei were stained with DAPI (blue). **b**, TUJ1 expression (intensity/area) is greater in r6-MO–treated SCOs than in untreated SCOs ($p$ = 0.0014, unpaired t-test; $n$ = 7 organoids from one SMA line). **c**, Representative images of TUNEL staining of Untr and r6-MO-treated SMA SCOs at 2 mo. Scale bar: 300 µm. Nuclei were stained with DAPI (blue). **d**, TUNEL-positive cells were less frequent in r6-MO–treated SCOs than in untreated SCOs ($p$ = 0.0192, unpaired t-test; $n$ = 4 organoids from one SMA cell line).

## SMA organoids exhibit aberrant electrical activity

Modifications in the electrophysiological activity of spinal MNs have previously been reported in 2D cultures[90] and pre-symptomatic mouse models of SMA[91]. As in other motor degenerative disorders[92], this abnormal activity might contribute to the SMA human disease phenotype along with MN death. However, it is not clear how early in the disease progression this dysfunction occurs and how it varies across CNS compartments. For the first time, we exploited high-density multi-electrode array (HD-MEA) technology to investigate the functionality of SCOs derived from SMA patients (**Fig. 11a**). Basal recordings of 2-month-old CTRL and SMA SCOs showed spontaneous spiking activity at low frequency, with lower frequencies in SMA SCOs (**Fig. 11b**). Moreover, SMA SCOs increased their firing frequency significantly more than CTRL SCOs after a glutamatergic stimulus, suggesting an early dysfunction with features of hyperexcitability (**Fig. 11c**). Treatment with r6-MO resulted in enhanced basal activity compared to untreated SMA SCOs (CTRL 1.926 ± 0.6211 Hz *vs*. SMA 1.251 ± 0.6043 Hz *vs.* r6-MO 1.576 ± 0.2848 Hz; $p = 0.0125$; **Fig. 11b**), which was paralleled by a reduced response to glutamatergic stimulus (percentage increase in frequency CTRL 48.36% ± 20.67 *vs*. SMA 95.00% ± 25.57, *vs*. r6-MO 49.35% ± 13.73; $p < 0.0001$; **Fig. 11c)**.

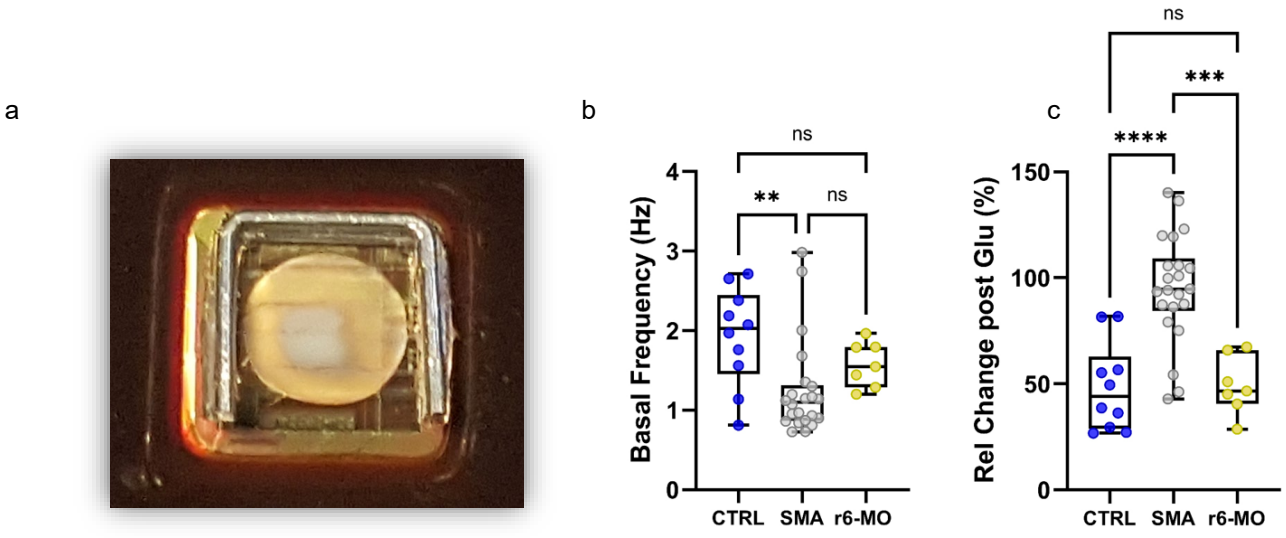

**Figure 11**. **SMA organoids display alterations in basal and evoked electrophysiological activity, which are rescued by MO treatment. a**, Representative picture of SCO on HD-MEA chip **b**, Basal firing activity was lower in SMA than in CTRL and r6-MO SCOs (ANOVA followed by Tukey post-hoc tests; $p = 0.0099$ (CTRL *vs* SMA), $p = 0.3942$ (SMA *vs* r6-MO); $p = 0.4330$ (CTRL *vs* r6-MO), $n \geq 7$ organoids from two CTRL and three SMA lines). **c**, The relative increase in firing frequency after glutamate (glu) perfusion was greater in SMA than in CTRL and r6-MO SCOs (ANOVA followed by Tukey post-hoc tests; $p < 0.0001$ (CTRL vs SMA), $p = 0.0001$ (SMA *vs* r6-MO); $p = 0.9958$ (CTRL *vs* r6-MO), $n \geq 7$ organoids from two CTRL and three SMA lines for the same organoids as in **c**).

Overall, we have shown that SCOs display a basal firing activity and the potential to respond to an exogenous stimulus. Furthermore, SMA SCOs possess distinct electrophysiological properties, including increased glutamate sensitivity. Taken together, these data provide novel insights into the value of optimized ASOs and their impacts in the treatment of SMA pathology.

## SMA cerebral organoids display pathological features.

SMA has traditionally been considered a lower MN disease; nonetheless, cerebral involvement has been reported in the most severe SMA cases[31]. However, it is still debatable whether this feature is to be directly linked to SMA pathogenesis or it is indirectly associated with the spinal degeneration. To begin exploring these alternatives, we employed an adapted protocol for generating 3D brain organoids[93] from SMA and healthy iPSC lines, where a putative secondary effect of spinal cord degeneration was excluded.

Both CTRL and SMA cerebral organoids displayed complex morphology, with staining for cortical neurons (CTIP2+ and SATB2+) at 2 months revealing the presence of different cell types (**12a**). Further, cerebral organoids displayed abnormal electrophysiological activity like that seen in the SMA SCO data. HD-MEA analysis (**Fig. 12b**) revealed that SMA cerebral organoids had a significantly lower basal spike frequency compared to CTRLs (0.806 ± 0.1652 Hz SMA vs. 2.397 ± 1.386 Hz CTRL, $p = 0.0039$.

Consistent with the SCO response observed after glutamatergic stimulation, SMA cerebral organoids increased their firing frequency by a significantly higher factor than CTRL organoids (189.4% ± 159 SMA vs. 50% ± 22.43 CTRL, $p = 0.0386$).

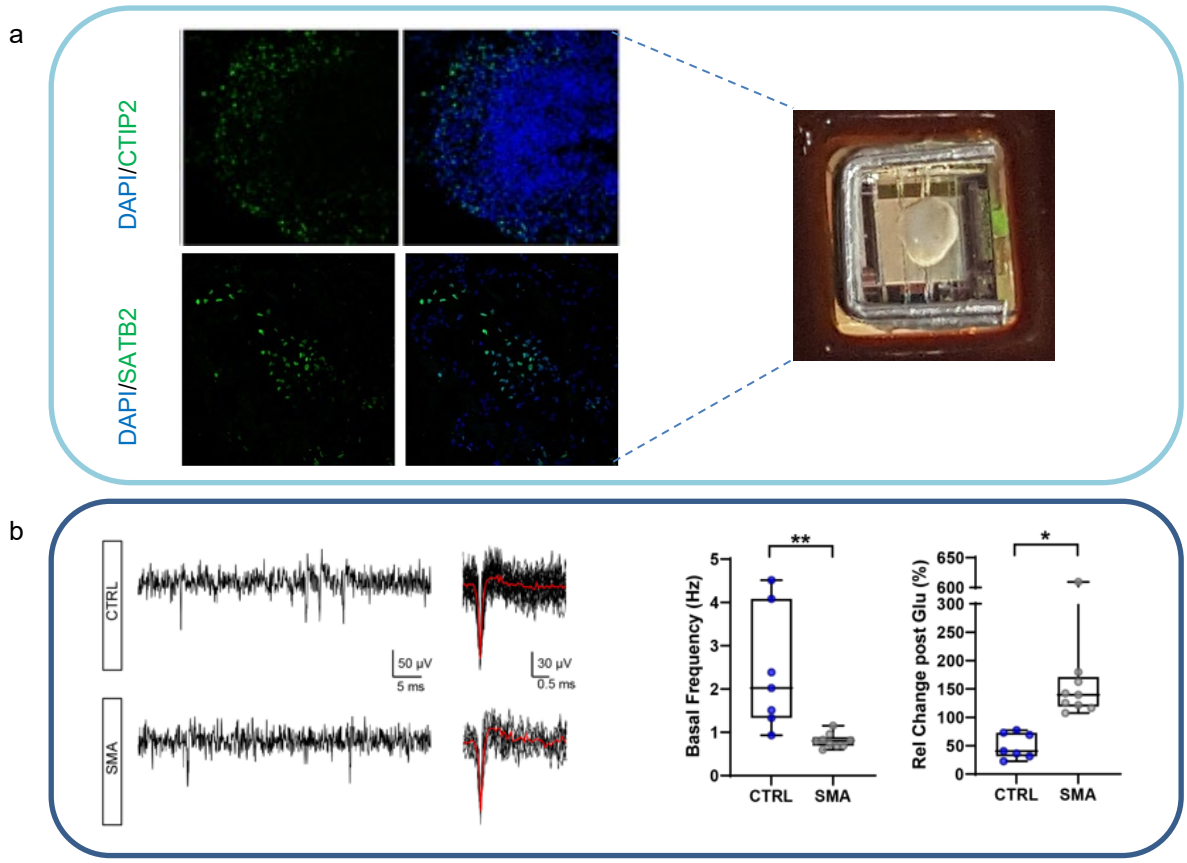


**Figure 12**. **SMA cerebral organoids display functional disease features. a** Representative image of immunostaining of markers for cortical neurons (CTIP2 and SATB2) in CTRL cerebral organoids at 2 mo. Nuclei were stained with DAPI (blue). Scale bar: 50 µm. **b,** Representative traces of basal recording of CTRL and SMA cerebral organoids (3 mo; left panel). Basal firing frequency was lower in SMA cerebral organoids than in CTRL organoids ($p = 0.0039$, unpaired *t*-test; $n \geq 7$ organoids from two CTRL and two SMA lines). The relative increase in firing frequency after glutamate (glu) perfusion was greater in SMA than in CTRL cerebral organoids ($p = 0.0386$, unpaired *t*-test) (right panel).

Our results thus show pathological features in SMA cerebral organoids, demonstrating direct involvement of the disease in the CNS, beyond the spinal cord, and highlight the need to consider additional targets in the clinical therapeutic setting to evaluate the efficacy and the long-term response to treatments.

# Discussion

Stem cell–based models of the human CNS provide an opportunity to unravel processes of human development and disease that could not otherwise be studied experimentally[94–96]. However, reproducing complex cell–cell interactions, circuit assembly, and human neurodegenerative features in conventional 2D culture remains a challenge [69]. Cerebral organoids have recently been proposed as a platform to study human development and identify disease phenotypes[68,97]. However, fewer descriptions of spinal cord organoids have been reported in the literature[66,98,99], and this area of research deserves further investigation in the context of MN diseases, neurological disorders with urgent unmet therapeutic needs. Here, we leveraged the organoid technology to generate SCOs and cerebral organoids from iPSCs of healthy subjects and SMA type 1 patients to further our understanding of SMA and testing innovative optimized therapies. This tool represents a significant advance beyond previous SMA 2D models in terms of recapitulating the development of physiological crosstalk between MN and other cell subpopulations.

The advent of disease-modifying therapies for SMA has changed the scenario of clinical practice and offered new expectations to patients, caregivers, and health care providers. Current evidence demonstrates that early treatment is essential for clinical efficacy. Thus, increased knowledge of the prenatal and pre-symptomatic stages of the disease is crucial to optimize therapeutic strategies. Even though SMA is a genetic disorder often with onset in newborns, very few studies have analyzed the prenatal stages of the disease, when SMN function is critical[100], and no human molecular data on SMA spinal cord at single-cell resolution have been reported thus far, exploring how different cell populations are affected. Prenatal MN cell death and dysfunction might condition the onset and severity of the disease postnatally and set the therapeutic window. Still largely unexplored is whether SMN deficiency impairs early

neuronal development and thereby triggers neuronal death. In this perspective, SMA organoids represent optimal substrates to be exploited to begin addressing the link between key early pathological features. Here, we demonstrated that both CTRL and SMA SCOs harbor a spectrum of spinal neuronal domains recapitulating the *in vivo* complexity of neuronal populations within the human developing spinal cord. Moreover, we showed that differentiation programs are affected in SMA spinal organoids. The developmental component of neurodegenerative disorder such as Huntington's disease has been recently confirmed [101,102] suggesting that this hypothesis can be investigated also in SMA.

The observation of reduced axonal length in SMA SCOs relative to CTRL demonstrates that the 3D model can reproduce key disease features of SMA. Intriguingly, early neuronal differentiation defects and apoptosis were reproduced in SMA SCOs, suggesting that concomitant defects in differentiation and increased degeneration could contribute to SMA pathogenesis.

A growing body of evidence suggests that SMA is a multifactorial disease in which the interaction of different cell types and disease mechanisms progressively leads to MN dysfunction and death[30,38,58]. Magnetic resonance imaging has revealed that severe SMA patients who survive beyond 1 year of age exhibit progressive and diffuse brain lesions[31]. Pre-natal spinal cord alterations have been reported in animal studies[38], and recently in humans[37]. A very recent study demonstrated functional alterations of the motor cortex and cerebellum in symptomatic SMA mice[103]. Herein, for the first time, we demonstrated that SMA cerebral organoids show impaired neuronal activity. This wider impact requires further characterization and needs to be considered for effective clinical management of SMA patients.

Indeed, the generation of spontaneous and evoked activity in both SCOs and brain organoids is impaired, supporting the biological relevance of the model and the direct impact that developmental alterations and/or plasticity events might cause on neuronal wiring.

Neuronal hyperexcitability has been described in the context of SMA[90,104] and amyotrophic lateral sclerosis (ALS)[105], associated with degeneration of both upper and lower MNs [92,106,107]. However, it is not clear how early in SMA progression this dysfunction arises and how it varies across CNS compartments. SMA SCOs showed decreased basal activity and hyperexcitability early on, likely contributing to the disease phenotypes. A growing body of literature leverages on CNS organoids to study the organization of human circuits also for the development of optimized therapeutic approaches[68,108]. As a future perspective, CNS organoids could provide a tool to study the organization of human neuronal circuits and the optimization of therapeutic approaches.

Single-cell sequencing of SMA SCOs revealed that they present a broad cellular composition, suggesting that SCOs could be used in the future to detect cell-autonomous and non-autonomous neuronal-specific vulnerabilities in other MN diseases. The reason for the specific vulnerability of MNs linked to reduced expression of SMN protein is still unclear. Interestingly, single-cell expression analysis highlighted, in particular in the MN subgroup, deregulated genes important for neuronal function, axonal growth, and synapsis formation, which were already described as altered in SMA or other neurological disorders. Among them, *synaptotagmin* and *neurexin* gene families are linked to neurotransmission impairment and MN vulnerability[76,81]. Intriguingly, *stathmin 2 (STMN2)*, mainly associated with neuronal growth and regeneration, was also identified as being deregulated. Alterations in its expression and molecular processing have already been described in other neurodegenerative disorders, as ALS and frontotemporal dementia[79,80,109], but not in SMA. These genes may contribute to the

selective MN dysfunction and represent a potential therapeutic target complementary to SMN. It will be intriguing to define whether early treatments can rescue these specific genes and act as neuroprotective signals for MNs in SMA.

The last decade has witnessed the development of a growing number of novel therapies for SMA. However, the FDA/EMA-approved treatment nusinersen[110], an ASO able to increase SMN expression by splicing correction of *SMN2*, requires administration by periodic lumbar puncture. Permeability of the blood–brain barrier and tissue distribution of ASO delivery can be fostered by CPPs, small cationic molecules with carrier capacity for macromolecular compounds. This strategy offers improved systemic distribution, including upon intravenous injection, in several disease models[89] and was proposed in the context of Duchenne muscular dystrophy[111]. A specific ASO with morpholino chemistry conjugated with the CPP r6 injected in symptomatic SMA mice *via* an intraperitoneal administration, provided results strikingly superior compared to unconjugated ASO in terms of survival, behavior and rescue of the pathological phenotype, suggesting that the peptide can successfully increase ASO biodistribution and efficiency[83]. In this study, for the first time, we tested the same conjugate in human tissue in SMA SCOs and demonstrated that the drug rescued SMA pathological hallmarks. Indeed, functional alterations were fully restored by the treatment, as well as apoptosis phenotype in SMA organoids. This not only opens new avenues of investigation to fully dissect the therapeutic mechanisms of action on the multifaceted aspects of SMA, but also confirms these novel models as suitable tools to improve the current therapeutic strategies in the clinic, and even expand to a more personalized medicine in the future.

Lastly, our study suggests that SMN is a key molecule during prenatal spinal cord and brain development, meaning that SMA therapeutics will be most effective if delivered during the

pre-symptomatic phase of the disorder, namely peri- or even prenatally. Further studies to analyze the multisystemic impact of SMN deficiency during development will be pivotal in defining the optimal therapeutic window and determining the efficacy of therapies on early developmental defects. There are also technical and ethical challenges related to *in utero* therapy that must be overcome before this new knowledge can be translated into clinical practice. Nevertheless, early developmental effects of SMA should be comprehensively discussed during prenatal counselling and whenever treatment is initiated. In any case, our data support the need for prompt treatment postnatally and the implementation of newborn screening.

Overall, our findings demonstrate that a human *in vitro* 3D model can successfully recapitulate early SMA pathological phenotypes in both the spinal cord and the brain. Remarkably, identified pathological hallmarks were rescued by innovative ASOs, suggesting that these SMA models can be used, and further exploited, for efficient and effective drug development.

# Materials and methods

## iPSC reprogramming and culture

The studies involving human samples were conducted in accordance with the ethical standards of the Declaration of Helsinki, national legislation, and institutional guidelines. Human fibroblast cell lines were obtained from Eurobiobank with informed consent, as approved by the ethical committee at Fondazione IRCCS Ca' Granda Ospedale Maggiore Policlinico and University of Milan (0004520). Fibroblasts derived from skin biopsies were reprogrammed into iPSCs using the CytoTune iPS 2.0 Kit (CytoTune-iPS Sendai 2.0 Reprogramming Kit, Invitrogen) and maintained in E8 (Essential 8™ Medium, Gibco, A1517001) medium at 37°C in 5% $CO_2$[ref.78].

## Generation of cerebral organoids

Cerebral organoids were generated by adapting a previous protocol[93]. IPSCs were harvested using Accutase (Life Technologies, A1110501) and approximately 9,000 iPSCs were plated in each well of an ultra-low attachment 96-well plate (Corning, CLS7007) in pluripotent stem cell media containing low recombinant human FGF-basic (4 ng/ml, Peprotech, 100-18B) and Y-27632 (50 μM ROCK inhibitor Calbiochem, 13624S). On day 6, obtained embryoid bodies (EBs) were transferred to low adhesion 24-well plates (Corning, CLS3473) in neural induction media (NIM) containing DMEM/F12 (Gibco, 11320033), 1% N2 supplement (Gibco, 17502001), 1% Glutamax (Life Technologies, 35050061), 1% MEM-NEAA (Gibco, 11140035), and 1 μg/ml heparin (Sigma, H3149). On day 12, the EBs were transferred to droplets of Cultrex® Basement Membrane Matrix Type 2 (BME type 2, Trevigen, 3532-001-02) and grown in differentiation media containing a 1:1 mixture of DMEM/F12 and Neurobasal (Gibco, 21103049) with 0.5% N2 supplement, 1% B27 supplement without vitamin A (Gibco,

12587010), 2-mercaptoethanol (ThermoFisher 21985023), 0.025% insulin (Sigma, I9278), 1% Glutamax, and 0.5% MEM-NEAA. After 2 days, the droplets were transferred to a spinning bioreactor containing the same media except B27 without vitamin A, which was replaced with B27 with vitamin A (Gibco, 17504044).

## Generation of spinal cord organoids (SCOs)

To generate SCOs, the same procedure described for human cerebral organoids was applied from day 0 to day 2. On day 2, half of the medium was changed to fresh medium containing a final concentration of 4 ng/ml bFGF, 50 μM Y-27632, 3 μM CHIR 99021 (GSK3 inhibitor, Sigma-Aldrich, SML1046), 2 μM SB-431542 (Activin/BMP/TGF-β pathway inhibitor, Sigma-Aldrich, S4317), and 0.2 μM LDN-193189 (inhibitor of the bone morphogenetic [BMP] pathway, Stemcell Technologies, 72149). On day 4, the medium was replaced, adding the same small molecules (excluding bFGF and Y-27632). On day 6, the EBs were transferred into ultra-low attachment 24-well plates and cultured in NIM plus 100 nM retinoic acid (RA, Sigma-Aldrich, R3255). On day 12 EBs embedded in Cultrex and cultured with SCO differentiation media (SCODM, composed by 1:1 DMEM/F12 and Neurobasal (Gibco, 21103049) with 0.5% N2 supplement, 1% B27, 2-mercaptoethanol (ThermoFisher 21985023), 0.025% insulin (Sigma, I9278), 1% Glutamax, and 0.5% MEM-NEAA). 1 μM Smoothened Agonist (SAG, Calbiochem, 364590-63-6) was added to the media. On day 14, SCOs were transferred to spinning bioreactors. On day 28, concentrations of RA and SAG were reduced to 50% and neurotrophic factors BDNF (Peprotech, 450-02), GDNF (Peprotech, 450-10), and IGF-1 (Sigma Aldrich, 100-12) were added at 10 ng/ml each.

## Immunohistochemistry analysis

Organoids were fixed with 4% paraformaldehyde (PFA) for 15 min at room temperature (RT) and subsequently placed in 30% sucrose/PBS overnight at 4°C. The next day, they were embedded in 10%-7.5% gelatin/sucrose, frozen in dry ice, placed at -80°C overnight, and cryosectioned to 20-µm sections using a cryostat. Organoid sections were permeabilized for 1 h in PBS with 0.3% Triton-X (Sigma) and 10% donkey or goat serum (Jackson ImmunoResearch) at RT.

2D cultures were fixed with 4% PFA at RT for 5 min and permeabilized in PBS with 0.2% Triton-X (Sigma) and 10% donkey or goat serum (Jackson ImmunoResearch) for 1 h at RT. Primary antibody diluted in fresh permeabilization solution was added overnight at 4°C (complete list summarized in **Table 1**). The following day, secondary antibodies (AlexaFluor 488, 555, 568, 594, and 647 conjugates, 1:1000; Invitrogen) were added with DAPI (1:500; Sigma-Aldrich, D9542) in PBS for 90 min at RT. DAKO mounting media (Agilent, S3023) was used to mount the coverslips. TUNEL assay was performed using a DeadEnd™ Fluorometric TUNEL System (Promega, G3250). Confocal images were obtained using a Leica SP8 white laser inverted confocal microscope (Leica) and analyzed using Fiji image-processing software.

## Image quantification

To evaluate the percentage of TUJ1-positive area, 10× mosaic images of whole cortical organoid sections were acquired using an Inverted Microscope DMi8 and the Leica LASX software platform. At least five different sections were acquired per organoid for at least 3 organoids/cell line for three CTRL and two SMA lines. In detail, a custom-designed ImageJ/Fiji[112] software image macro was applied to evaluate the proportion of $TUJ1^+$ area (as %). For TUNEL quantification, images were acquired by an inverted Nikon-Crest multimodal

spinning-disk confocal microscope. Quantification of nuclei (DAPI) and TUNEL-positive cells was performed with an *ad-hoc* designed analysis pipeline for thresholding and segmentation using the GA2 module in Nis-Elements v5.21 software (Nikon-Lim Instruments). Regarding neurofilament tracing, images previously acquired with a Leica SP8 white laser inverted confocal microscope (Leica) were analyzed using Fiji image-processing software. The NeuronJ plug-in was used for the tracing and analysis of axon length.

## Quantitative real-time PCR (qRT-PCR)

Total RNA was extracted using the ReliaPrep RNA Cell Miniprep System (Promega, Z6010). The RNA concentration was tested using Nanodrop (Thermo Fisher Scientific). Reverse transcription was performed using SuperScript IV VILO Master Mix (Thermo Fisher Scientific). 150 ng of template total RNA were retrotranscripted. The expression level of candidate genes (**Table 2**) was assessed by TaqMan quantitative analysis on the 7500 Real-Time PCR System and 7900HT Fast Real-Time PCR System (Applied Biosystem), GAPDH was used as a reference gene. The ΔΔCt method was used to calculate gene expression[113].

## Electrophysiology.

High-density multielectrode array (HD-MEA) was used to record the extracellular spontaneous activity of both SCOs and cerebral organoids. The device consists of 4096 planar electrodes measuring 21 μm × 21 μm, covering an area of 2.67 mm × 2.67 mm (Biocam X with Biochip Arena, 3Brain AG, Swiss). Organoids were gently positioned on the chip and fixed with a platinum anchor and a nylon mesh. Before and during recordings, organoids were submerged in Kreb's solution with the following composition (mM): 120 NaCl, 2 KCl, 1.19 $MgSO_4$, 26 $NaHCO_3$, 1.18 $KH_2PO_4$, 11 glucose, 2 $CaCl_2$, oxygenated with a mix of 95% $O_2$/5% $CO_2$ to obtain pH 7.4. Organoids were recorded under control conditions for 15 min, after addition of 100 μM of glutamate (L-glutamic acid, Sigma-Aldrich) for an additional 15 min, and after adding the combination of 100 μM glutamate, 10 μM gabazine (SR-95531, Abcam), and 1M strychnine hydrochloride (Sigma-Aldrich) for an additional 15 min. Brainwave X (3Brain AG) software was used to record the electrophysiological activity at the sampling frequency of 17 kHz. Brainwave 4 software (3Brain AG) was used to analyze the traces offline. The precise time spike detection (PTSD) algorithm was used to detect the spikes (parameters used: positive and negative peak, peak duration <1 ms, refractory period >1 ms, and detection threshold >7 times the standard deviation of the noise). Spike sorting was performed using a principal component analysis with K-means (silhouette method) considering a maximum three clusters per electrode and three spikes per cluster. These findings were also confirmed by re-analyzing the signals and removing any confounders; only channels showing stable activity during the control period (without fluctuations exceeding 20% spike frequency) were taken into consideration.

## Morpholino treatment

We used a morpholino (MO)10-34 sequence targeting the SMN2 ISS-N1 region downstream of exon 7 that was previously described by our lab[88]. MO was conjugated with r6 peptide (r6-MO). MO oligomers were synthesized by Gene Tools. We treated SMA SCOs with growing concentrations of r6-MO. The solution containing 2.4 nmoles r6-MO was added directly to each well and incubated for 48h. Afterwards, the culture medium was changed and fresh aliquots of 2.4 nmoles r6-MO added for an additional 48 h. The medium was then replaced with fresh medium for 72 h. Lastly, the organoids were treated again with 4.8 nmoles of r6-MO for 48 h.

## Western blot analysis

Western blot analysis was performed as described previously[88]. Briefly, samples were sonicated in lysis buffer supplemented with protease and phosphatase inhibitors (Pierce Rockford, IL, USA) on ice for 10 min. Approximately 5 µg of protein was separated by 12% SDS-PAGE and electrophoretically transferred to a nitrocellulose membrane. The membranes were incubated with anti-SMN (1:1000, BD) and anti-actin (1:1000, Sigma, St. Louis, MO, USA) antibodies. After labeling with peroxidase-conjugated secondary antibody (Life Technologies), the proteins were detected using a chemiluminescent substrate (Amersham, Pittsburgh, PA, USA). Densitometry analysis was performed using Image Studio Lite ver. 5.2.

## 2D culture of cells from dissociated organoids

SCOs were centrifuged at 300*g* for 5 min and trypsin-EDTA was added before transferring organoids in the water bath at 37°C for 5 min. The organoids were then mechanically dissociated, and a double volume of horse serum (Euroclone, ECS0091L) used to inactivate

the trypsin before centrifugation. The supernatant was discarded, and SCO differentiation media was employed to resuspend the pellet. Approximately 50,000 cells were seeded in 24-well plates with coverslips previously coated with poly-L-ornithine (Sigma-Aldrich, P3655) and laminin (Sigma-Aldrich, L2020). SCO differentiation media supplemented with RA, SAG, and growth factors at the same concentration of differentiation day 28, was used for the maintenance of organoid-derived cells.

## SCO cell dissociation for scRNA sequencing analysis

2 mo SCOs were individually dissociated and separately processed for scRNA sequencing. Dissociation was performed using an optimized protocol based on the Worthington Papain Dissociation System Kit (Worthington Biochemical). Single cell suspensions were collected on ice-cold PBS (without calcium and magnesium) with 0.04% BSA (Sigma Aldrich) at $1\times10^6$/ml as counted by an automatic cell counter (Countess II, Thermo Fisher).

## Single-cell RNA-sequencing

Approximately 8000 cells from each sample prepared as described above were loaded into one channel of the Single Cell Chip B using the Single Cell 3' v3 reagent kit (10X Genomics) for gel bead emulsion generation in the Chromium system. Following capture and lysis, cDNA was synthesized and amplified for 14 cycles following the manufacturer's protocol (10X Genomics). The amplified cDNA (50 ng) was then used for each sample to construct Illumina sequencing libraries. Sequencing was performed on the NextSeq550 Illumina sequencing platform following the 10x Genomics instructions for read generation. A sequencing depth of ~45,000 reads/cell was obtained for each sample.

## Mapping and extraction of single-cell mRNA transcript counts

Raw sequencing data (bcl-files) were converted to fastq files using the Illumina bcl2fastq tool integrated into the CellRanger (10X Genomics) suite (version 3.0.2). The CellRanger analysis pipeline was used to generate a digital gene expression matrix starting from raw data. Reads were aligned to the human GRCh38 reference genome and annotated and counted with gene annotations from Ensembl version 93. The CellRanger count module was used to map reads with default settings, and the sequence length was set to r1-length=28 and -r2-length=55. At least 90,000 reads per cell were produced. The 32 raw digital gene expression matrix (unique molecular identifiers [UMIs] per gene per cell) was imported in R (https://www.Rproject.org/) version 3.6.3 using the Seurat R package (version 3.1.1). Briefly, the UMI counts per gene per cell for each biological replicate were imported into Seurat. Quality control of 2 mo SCOs was assessed by filtering out cells meeting any of the following criteria: <200 unique genes expressed, <300UMIs, or >25% of reads mapping to mitochondria. Raw data were normalized through a global-scaling method, converted by a scale factor (10,000 by default), and log-transformed. Scaling the data and removing unwanted sources of variation were achieved through the ScaleData Seurat function.

## Single-cell data analysis

Cell cycle scores were calculated using cell cycle genes and used to regress out cell cycle effects. Variable genes across single cells in each sample were detected by principal component analysis (PCA). Data from each sample were integrated using the first 100 dimensions. After aligning subspaces, clustering was performed by the FindClusters function using the first 71 dimensions as computed by the JackStraw function. Uniform manifold approximation and projection (UMAP) dimensional reduction was computed by the RunUMAP function. FindClusters with a resolution parameter of 0.3. Finally, clusters were manually curated and

annotated based on markers available in the literature. Marker genes for each cluster were defined with the function FindAllMarkers with standard parameters.

The pipeline for data visualization was adapted from https://github.com/crickbabs/ZebrafishDevelopingHindbrainAtlas[114].

The module enrichment score was computed by running AddModuleScore() function from Seurat package using as input different manually curated and annotated marker gene lists for each cell type based on markers available in the literature[66,115,116].

## Identification of differentially expressed genes between 2mo CTRL and SMA SCOs

Single-cell RNA sequencing differential gene expression analysis was performed with Seurat (version Seurat 3.1.1) and it is based on non-parametric Wilcoxon rank sum test. Genes were considered significantly differentially expressed between SMA and CTRL if they had an absolute log fold change ≥0.2, min.pct= 0.25 and adjusted p-value <0.05.

Pathway enrichment analysis was carried on differentially expressed genes in selected clusters by mapping functional Reactome pathways annotation collection using gProfiler as previously described[117]. The resulting enrichment results were visualized with the Enrichment Map plugin for the Cytoscape 3.8.0 network visualization and analysis software[118]. We loaded gProfiler results using an FDR cut-off of 0.05. In the map, each gene set is symbolized by a node in the network. Node size corresponds to the number of genes comprising the gene-set. To intuitively identify redundancies between gene sets, the nodes are connected with edges if their contents overlap by more than 50%. The thickness of the edge corresponds to the size of the overlap.

## Statistical analysis

Continuous variables were analyzed through descriptive statistics and reported as mean±SD. Differences between groups and changes with respect to baseline were assessed by unpaired and paired t-test as appropriate. Comparisons of more than two groups were carried out with one-way or two-way ANOVA as appropriate; follow-up tests for multiple comparisons (Tukey HSD or Sidak's test) were used in case of significant differences. All p-values were two-sided and significance assumed at the 5% level of probability. GraphPad Prism v.8 was used for all analyses.

## Table 1. Primary antibodies.

| Antibody | Dilution | Cat # | Vendor |
|---|---|---|---|
| Sex-determining region Y-box 2 (SOX2) | 1:500 | ab97959 | Abcam |
| BIII tubulin (TUJ1) | 1:500 | 801201 | Biolegend |
| Microtubule-associated protein 2 (MAP2) | 1:100 | M9942 | Sigma Aldrich |
| Doublecortin (DCX) | 1:1000 | ab18723 | Abcam |
| Special AT-rich sequence-binding protein 2 (SATB2) | 1:100 | ab51502 | Abcam |
| Glial fibrillary acidic protein (GFAP) | 1:100 | G3893 | Sigma |
| Neurofilament H (SMI32) | 1:500 | 801701 | Biolegend |
| Oligodendrocyte transcription factor (OLIG2) | 1:100 | SAB1404798 | Sigma |
| Paired box protein 6 (PAX6) | 1:100 | 42660 | Invitrogen |
| S100 calcium-binding protein (S100b) | 1:100 | ab52642 | Abcam |
| Nestin | 1:100 | ab27952 | Abcam |
| CTIP2 | 1:100 | ab18465 | Abcam |
| Recombinant anti-ISLET 1 | 1:100 | ab109517 | Abcam |
| Hoxb4 | 1:100 | ab133521 | Abcam |
| Goat 555 anti-mouse IgM TRA-1-60 | 1:500 | A24871 | Molecular Probes |

## Table 2. qPCR probes.

TaqMan probes.

| Acronym | Definition | Probe |
|---|---|---|
| CHAT | Choline O-acetyltransferase | Hs00252848_m1 |
| ISL1 | Islet 1 | Hs00158126_m1 |
| OLIG2 | Oligodendrocyte transcription factor 2 | Hs00300164_s1 |
| SOX2 | Sex-determining region Y (SRY)-box 2 | Hs01053049_s1 |
| POU5F1 (OCT4) | Transcription factor with POU domain | Hs00742896_s1 |
| MAP2 | Microtubule-associated protein tau | Hs00258900_m1 |
| HB9 | Homeobox protein HB9 | Hs00232128_m1 |
| TUJ1 | Neuron-specific class III β-tubulin | Hs00801390_s1 |
| GAPDH | Glyceraldehyde-3-phosphate dehydrogenase | Hs99999905_m1 |

# References


1. Werdnig G. Two early infantile hereditary cases of progressive muscular atrophy simulating dystrophy, but on a neural basis. 1891. *Arch Neurol*. 1971;25(3):276-278.

2. Fidziańska A. Ultrastructural changes in muscle in spinal muscular atrophy. Werding-Hoffmann's disease. *Acta Neuropathol*. 1974;27(3):247-256.

3. Lorson CL, Hahnen E, Androphy EJ, Wirth B. A single nucleotide in the SMN gene regulates splicing and is responsible for spinal muscular atrophy. *Proc Natl Acad Sci USA*. 1999;96(11):6307-6311. doi:10.1073/pnas.96.11.6307

4. Le TT, Pham LT, Butchbach MER, et al. SMNΔ7, the major product of the centromeric survival motor neuron (SMN2) gene, extends survival in mice with spinal muscular atrophy and associates with full-length SMN. *Hum Mol Genet*. 2005;14(6):845-857. doi:10.1093/hmg/ddi078

5. Elsheikh B, Prior T, Zhang X, et al. An analysis of disease severity based on SMN2 copy number in adults with spinal muscular atrophy. *Muscle Nerve*. 2009;40(4):652-656. doi:10.1002/mus.21350

6. Feldkötter M, Schwarzer V, Wirth R, Wienker TF, Wirth B. Quantitative analyses of SMN1 and SMN2 based on real-time lightCycler PCR: fast and highly reliable carrier testing and prediction of severity of spinal muscular atrophy. *Am J Hum Genet*. 2002;70(2):358-368. doi:10.1086/338627

7. Prior TW, Swoboda KJ, Scott HD, Hejmanowski AQ. Homozygous SMN1 deletions in unaffected family members and modification of the phenotype by SMN2. *Am J Med Genet A*. 2004;130A(3):307-310. doi:10.1002/ajmg.a.30251

8. Schrank B, Götz R, Gunnersen JM, et al. Inactivation of the survival motor neuron gene, a candidate gene for human spinal muscular atrophy, leads to massive cell death in early mouse embryos. *Proc Natl Acad Sci USA*. 1997;94(18):9920-9925.

9. Monani UR, Sendtner M, Coovert DD, et al. The human centromeric survival motor neuron gene (SMN2) rescues embryonic lethality in Smn(-/-) mice and results in a mouse with spinal muscular atrophy. *Hum Mol Genet*. 2000;9(3):333-339.

10. Bevan AK, Hutchinson KR, Foust KD, et al. Early heart failure in the SMNDelta7 model of spinal muscular atrophy and correction by postnatal scAAV9-SMN delivery. *Hum Mol Genet*. 2010;19(20):3895-3905. doi:10.1093/hmg/ddq300

11. Butchbach MER, Edwards JD, Schussler KR, Burghes AHM. A novel method for oral delivery of drug compounds to the neonatal SMNΔ7 mouse model of spinal muscular atrophy. *J Neurosci Methods*. 2007;161(2):285-290. doi:10.1016/j.jneumeth.2006.11.002

12. Dominguez E, Marais T, Chatauret N, et al. Intravenous scAAV9 delivery of a codon-optimized SMN1 sequence rescues SMA mice. *Hum Mol Genet*. 2011;20(4):681-693. doi:10.1093/hmg/ddq514

13. Cherry JJ, Osman EY, Evans MC, et al. Enhancement of SMN protein levels in a mouse model of spinal muscular atrophy using novel drug-like compounds. *EMBO Mol Med*. 2013;5(7):1035-1050. doi:10.1002/emmm.201202305

14. Wang J, Dreyfuss G. A cell system with targeted disruption of the SMN gene: functional conservation of the SMN protein and dependence of Gemin2 on SMN. *J Biol Chem*. 2001;276(13):9599-9605. doi:10.1074/jbc.M009162200

15. Burghes AHM, Beattie CE. Spinal muscular atrophy: why do low levels of survival motor neuron protein make motor neurons sick? *Nat Rev Neurosci*. 2009;10(8):597-609. doi:10.1038/nrn2670

16. Gabanella F, Butchbach MER, Saieva L, Carissimi C, Burghes AHM, Pellizzoni L. Ribonucleoprotein assembly defects correlate with spinal muscular atrophy severity and preferentially affect a subset of spliceosomal snRNPs. *PLoS ONE*. 2007;2(9):e921. doi:10.1371/journal.pone.0000921

17. Tisdale S, Pellizzoni L. Disease mechanisms and therapeutic approaches in spinal muscular atrophy. *J Neurosci*. 2015;35(23):8691-8700. doi:10.1523/JNEUROSCI.0417-15.2015

18. Donlin-Asp PG, Bassell GJ, Rossoll W. A role for the survival of motor neuron protein in mRNP assembly and transport. *Curr Opin Neurobiol*. 2016;39:53-61. doi:10.1016/j.conb.2016.04.004

19. Sleigh JN, Gillingwater TH, Talbot K. The contribution of mouse models to understanding the pathogenesis of spinal muscular atrophy. *Dis Model Mech*. 2011;4(4):457-467. doi:10.1242/dmm.007245

20. Hsieh-Li HM, Chang JG, Jong YJ, et al. A mouse model for spinal muscular atrophy. *Nat Genet*. 2000;24(1):66-70. doi:10.1038/71709

21. Monani UR, Coovert DD, Burghes AH. Animal models of spinal muscular atrophy. *Hum Mol Genet*. 2000;9(16):2451-2457. doi:10.1093/hmg/9.16.2451

22. Mentis GZ, Blivis D, Liu W, et al. Early functional impairment of sensory-motor connectivity in a mouse model of spinal muscular atrophy. *Neuron*. 2011;69(3):453-467. doi:10.1016/j.neuron.2010.12.032

23. Fletcher EV, Simon CM, Pagiazitis JG, et al. Reduced sensory synaptic excitation impairs motor neuron function via Kv2.1 in spinal muscular atrophy. *Nat Neurosci*. 2017;20(7):905-916. doi:10.1038/nn.4561

24. Kariya S, Mauricio R, Dai Y, Monani UR. The neuroprotective factor Wld(s) fails to mitigate distal axonal and neuromuscular junction (NMJ) defects in mouse models of spinal muscular atrophy. *Neurosci Lett*. 2009;449(3):246-251. doi:10.1016/j.neulet.2008.10.107

25. Ruiz R, Casañas JJ, Torres-Benito L, Cano R, Tabares L. Altered intracellular Ca2+ homeostasis in nerve terminals of severe spinal muscular atrophy mice. *J Neurosci*. 2010;30(3):849-857. doi:10.1523/JNEUROSCI.4496-09.2010

26. Kong L, Wang X, Choe DW, et al. Impaired synaptic vesicle release and immaturity of neuromuscular junctions in spinal muscular atrophy mice. *J Neurosci*. 2009;29(3):842-851. doi:10.1523/JNEUROSCI.4434-08.2009

27. Hunter G, Aghamaleky Sarvestany A, Roche SL, Symes RC, Gillingwater TH. SMN-dependent intrinsic defects in Schwann cells in mouse models of spinal muscular atrophy. *Hum Mol Genet*. 2014;23(9):2235-2250. doi:10.1093/hmg/ddt612

28. Hua Y, Sahashi K, Rigo F, et al. Peripheral SMN restoration is essential for long-term rescue of a severe spinal muscular atrophy mouse model. *Nature*. 2011;478(7367):123-126. doi:10.1038/nature10485

29. Shababi M, Habibi J, Yang HT, Vale SM, Sewell WA, Lorson CL. Cardiac defects contribute to the pathology of spinal muscular atrophy models. *Hum Mol Genet*. 2010;19(20):4059-4071. doi:10.1093/hmg/ddq329

30. Yeo CJJ, Darras BT. Overturning the Paradigm of Spinal Muscular Atrophy as Just a Motor Neuron Disease. *Pediatr Neurol*. 2020;109:12-19. doi:10.1016/j.pediatrneurol.2020.01.003

31. Mendonça RH, Rocha AJ, Lozano-Arango A, et al. Severe brain involvement in 5q spinal muscular atrophy type 0. *Ann Neurol*. 2019;86(3):458-462. doi:10.1002/ana.25549

32. Harding BN, Kariya S, Monani UR, et al. Spectrum of neuropathophysiology in spinal muscular atrophy type I. *J Neuropathol Exp Neurol*. 2015;74(1):15-24. doi:10.1097/NEN.0000000000000144

33. Soler-Botija C, Ferrer I, Gich I, Baiget M, Tizzano EF. Neuronal death is enhanced and begins during foetal development in type I spinal muscular atrophy spinal cord. *Brain*. 2002;125(Pt 7):1624-1634. doi:10.1093/brain/awf155

34. Burlet P, Huber C, Bertrandy S, et al. The distribution of SMN protein complex in human fetal tissues and its alteration in spinal muscular atrophy. *Hum Mol Genet*. 1998;7(12):1927-1933. doi:10.1093/hmg/7.12.1927

35. Ikemoto A, Hirano A, Matsumoto S, Akiguchi I, Kimura J. Synaptophysin expression in the anterior horn of Werdnig-Hoffmann disease. *J Neurol Sci*. 1996;136(1-2):94-100. doi:10.1016/0022-510x(95)00297-f

36. Yamanouchi Y, Yamanouchi H, Becker LE. Synaptic alterations of anterior horn cells in Werdnig-Hoffmann disease. *Pediatr Neurol*. 1996;15(1):32-35. doi:10.1016/0887-8994(96)00123-3

37. Kong L, Valdivia DO, Simon CM, et al. Impaired prenatal motor axon development necessitates early therapeutic intervention in severe SMA. *Sci Transl Med*. 2021;13(578):eabb6871. doi:10.1126/scitranslmed.abb6871

38. Motyl AAL, Faller KME, Groen EJN, et al. Pre-natal manifestation of systemic developmental abnormalities in spinal muscular atrophy. *Hum Mol Genet*. doi:10.1093/hmg/ddaa146

39. Lally C, Jones C, Farwell W, Reyna SP, Cook SF, Flanders WD. Indirect estimation of the prevalence of spinal muscular atrophy Type I, II, and III in the United States. *Orphanet J Rare Dis*. 2017;12(1):175. doi:10.1186/s13023-017-0724-z

40. Verhaart IEC, Robertson A, Wilson IJ, et al. Prevalence, incidence and carrier frequency of 5q–linked spinal muscular atrophy – a literature review. *Orphanet J Rare Dis*. 2017;12. doi:10.1186/s13023-017-0671-8

41. Munsat TL, Davies KE. International SMA consortium meeting. (26-28 June 1992, Bonn, Germany). *Neuromuscul Disord*. 1992;2(5-6):423-428.

42. Mercuri E, Bertini E, Iannaccone ST. Childhood spinal muscular atrophy: controversies and challenges. *Lancet Neurol*. 2012;11(5):443-452. doi:10.1016/S1474-4422(12)70061-3

43. Wang CH, Finkel RS, Bertini ES, et al. Consensus statement for standard of care in spinal muscular atrophy. *J Child Neurol*. 2007;22(8):1027-1049. doi:10.1177/0883073807305788

44. Rudnik-Schöneborn S, Heller R, Berg C, et al. Congenital heart disease is a feature of severe infantile spinal muscular atrophy. *J Med Genet*. 2008;45(10):635-638. doi:10.1136/jmg.2008.057950

45. Palladino A, Passamano L, Taglia A, et al. Cardiac involvement in patients with spinal muscular atrophies. *Acta Myol*. 2011;30(3):175-178.

46. Kaufmann P, McDermott MP, Darras BT, et al. Observational study of spinal muscular atrophy type 2 and 3: functional outcomes over 1 year. *Arch Neurol*. 2011;68(6):779-786. doi:10.1001/archneurol.2010.373

47. Yuan P, Jiang L. Clinical characteristics of three subtypes of spinal muscular atrophy in children. *Brain Dev*. Published online September 5, 2014. doi:10.1016/j.braindev.2014.08.007

48. Piepers S, van den Berg LH, Brugman F, et al. A natural history study of late onset spinal muscular atrophy types 3b and 4. *J Neurol*. 2008;255(9):1400-1404. doi:10.1007/s00415-008-0929-0

49. Prior TW, Nagan N, Sugarman EA, Batish SD, Braastad C. Technical standards and guidelines for spinal muscular atrophy testing. *Genet Med*. 2011;13(7):686-694. doi:10.1097/GIM.0b013e318220d523

50. Rudnik–Schöneborn S, Eggermann T, Kress W, Lemmink HH, Cobben JM, Zerres K. Clinical utility gene card for: proximal spinal muscular atrophy. *Eur J Hum Genet*. 2012;20(6). doi:10.1038/ejhg.2012.62

51. Lefebvre S, Bürglen L, Reboullet S, et al. Identification and characterization of a spinal muscular atrophy-determining gene. *Cell*. 1995;80(1):155-165.

52. Arnold WD, Kassar D, Kissel JT. Spinal muscular atrophy: Diagnosis and management in a new therapeutic era. *Muscle Nerve*. Published online October 24, 2014. doi:10.1002/mus.24497

53. Ogino S, Wilson RB. Genetic testing and risk assessment for spinal muscular atrophy (SMA). *Hum Genet*. 2002;111(6):477-500. doi:10.1007/s00439-002-0828-x

54. Kariyawasam DST, Russell JS, Wiley V, Alexander IE, Farrar MA. The implementation of newborn screening for spinal muscular atrophy: the Australian experience. *Genet Med*. Published online October 14, 2019. doi:10.1038/s41436-019-0673-0

55. Scully MA, Farrell PM, Ciafaloni E, Griggs RC, Kwon JM. Cystic fibrosis newborn screening: A model for neuromuscular disease screening? *Ann Neurol*. Published online November 26, 2014. doi:10.1002/ana.24316

56. Swoboda KJ. SMN-targeted therapeutics for spinal muscular atrophy: are we SMArt enough yet? *J Clin Invest*. 2014;124(2):487-490. doi:10.1172/JCI74142

57. Mercuri E, Pera MC, Scoto M, Finkel R, Muntoni F. Spinal muscular atrophy - insights and challenges in the treatment era. *Nat Rev Neurol*. 2020;16(12):706-715. doi:10.1038/s41582-020-00413-4

58. Faravelli I, Corti S. Spinal muscular atrophy - challenges in the therapeutic era. *Nat Rev Neurol*. 2020;16(12):655-656. doi:10.1038/s41582-020-00411-6

59. Tiziano FD, Tizzano EF. 25 years of the SMN genes: the Copernican revolution of spinal muscular atrophy. *Acta Myol*. 2020;39(4):336-344. doi:10.36185/2532-1900-037

60. Takahashi K, Tanabe K, Ohnuki M, et al. Induction of pluripotent stem cells from adult human fibroblasts by defined factors. *Cell*. 2007;131(5):861-872. doi:10.1016/j.cell.2007.11.019

61. Lancaster MA, Knoblich JA. Generation of cerebral organoids from human pluripotent stem cells. *Nat Protoc*. 2014;9(10):2329-2340. doi:10.1038/nprot.2014.158

62. Kadoshima T, Sakaguchi H, Nakano T, et al. Self-organization of axial polarity, inside-out layer pattern, and species-specific progenitor dynamics in human ES cell-derived neocortex. *Proc Natl Acad Sci U S A*. 2013;110(50):20284-20289. doi:10.1073/pnas.1315710110

63. Lancaster MA, Renner M, Martin CA, et al. Cerebral organoids model human brain development and microcephaly. *Nature*. 2013;501(7467):373-379. doi:10.1038/nature12517

64. Nakano T, Ando S, Takata N, et al. Self-formation of optic cups and storable stratified neural retina from human ESCs. *Cell Stem Cell*. 2012;10(6):771-785. doi:10.1016/j.stem.2012.05.009

65. Sakaguchi H, Kadoshima T, Soen M, et al. Generation of functional hippocampal neurons from self-organizing human embryonic stem cell-derived dorsomedial telencephalic tissue. *Nat Commun*. 2015;6:8896. doi:10.1038/ncomms9896

66. Andersen J, Revah O, Miura Y, et al. Generation of Functional Human 3D Cortico-Motor Assembloids. *Cell*. 2020;183(7):1913-1929.e26. doi:10.1016/j.cell.2020.11.017

67. Quadrato G, Brown J, Arlotta P. The promises and challenges of human brain organoids as models of neuropsychiatric disease. *Nat Med*. 2016;22(11):1220-1228. doi:10.1038/nm.4214

68. Paulsen B, Velasco S, Kedaigle AJ, et al. Autism genes converge on asynchronous development of shared neuron classes. *Nature*. 2022;602(7896):268-273. doi:10.1038/s41586-021-04358-6

69. Faravelli I, Costamagna G, Tamanini S, Corti S. Back to the origins: Human brain organoids to investigate neurodegeneration. *Brain Res*. 2020;1727:146561. doi:10.1016/j.brainres.2019.146561

70. d'Errico P, Boido M, Piras A, et al. Selective vulnerability of spinal and cortical motor neuron subpopulations in delta7 SMA mice. *PLoS ONE*. 2013;8(12):e82654. doi:10.1371/journal.pone.0082654

71. Mendonça RH, Rocha AJ, Lozano-Arango A, et al. Severe brain involvement in 5q spinal muscular atrophy type 0. *Ann Neurol*. 2019;86(3):458-462. doi:10.1002/ana.25549

72. Sagner A, Briscoe J. Establishing neuronal diversity in the spinal cord: a time and a place. *Development*. 2019;146(22). doi:10.1242/dev.182154

73. Lupo G, Harris WA, Lewis KE. Mechanisms of ventral patterning in the vertebrate nervous system. *Nat Rev Neurosci*. 2006;7(2):103-114. doi:10.1038/nrn1843

74. Amoroso MW, Croft GF, Williams DJ, et al. Accelerated high-yield generation of limb-innervating motor neurons from human stem cells. *J Neurosci*. 2013;33(2):574-586. doi:10.1523/JNEUROSCI.0906-12.2013

75. Du ZW, Chen H, Liu H, et al. Generation and expansion of highly pure motor neuron progenitors from human pluripotent stem cells. *Nat Commun*. 2015;6:6626. doi:10.1038/ncomms7626

76. Rizzo F, Nizzardo M, Vashisht S, et al. Key role of SMN/SYNCRIP and RNA-Motif 7 in spinal muscular atrophy: RNA-Seq and motif analysis of human motor neurons. *Brain*. 2019;142(2):276-294. doi:10.1093/brain/awy330

77. Akten B, Kye MJ, Hao LT, et al. Interaction of survival of motor neuron (SMN) and HuD proteins with mRNA cpg15 rescues motor neuron axonal deficits. *Proc Natl Acad Sci U S A*. 2011;108(25):10337-10342. doi:10.1073/pnas.1104928108

78. Corti S, Nizzardo M, Simone C, et al. Genetic correction of human induced pluripotent stem cells from patients with spinal muscular atrophy. *Sci Transl Med*. 2012;4(165):165ra162. doi:10.1126/scitranslmed.3004108

79. Klim JR, Williams LA, Limone F, et al. ALS-implicated protein TDP-43 sustains levels of STMN2, a mediator of motor neuron growth and repair. *Nat Neurosci*. 2019;22(2):167-179. doi:10.1038/s41593-018-0300-4

80. Melamed Z, López-Erauskin J, Baughn MW, et al. Premature polyadenylation-mediated loss of stathmin-2 is a hallmark of TDP-43-dependent neurodegeneration. *Nat Neurosci*. 2019;22(2):180-190. doi:10.1038/s41593-018-0293-z

81. Nizzardo M, Taiana M, Rizzo F, et al. Synaptotagmin 13 is neuroprotective across motor neuron diseases. *Acta Neuropathol*. 2020;139(5):837-853. doi:10.1007/s00401-020-02133-x

82. Nizzardo M, Simone C, Salani S, et al. Effect of combined systemic and local morpholino treatment on the spinal muscular atrophy Δ7 mouse model phenotype. *Clin Ther*. 2014;36(3):340-356.e5. doi:10.1016/j.clinthera.2014.02.004

83. Bersani M, Rizzuti M, Pagliari E, et al. Cell-penetrating peptide-conjugated Morpholino rescues SMA in a symptomatic preclinical model. *Mol Ther*. Published online November 19, 2021:S1525-0016(21)00583-9. doi:10.1016/j.ymthe.2021.11.012

84. Foged C, Nielsen HM. Cell-penetrating peptides for drug delivery across membrane barriers. *Expert Opin Drug Deliv*. 2008;5(1):105-117. doi:10.1517/17425247.5.1.105

85. Lebleu B, Moulton HM, Abes R, et al. Cell penetrating peptide conjugates of steric block oligonucleotides. *Adv Drug Deliv Rev*. 2008;60(4-5):517-529. doi:10.1016/j.addr.2007.09.002

86. Amantana A, Moulton HM, Cate ML, et al. Pharmacokinetics, biodistribution, stability and toxicity of a cell-penetrating peptide-morpholino oligomer conjugate. *Bioconjug Chem*. 2007;18(4):1325-1331. doi:10.1021/bc070060v

87. Moulton HM, Moulton JD. Morpholinos and their peptide conjugates: therapeutic promise and challenge for Duchenne muscular dystrophy. *Biochim Biophys Acta*. 2010;1798(12):2296-2303. doi:10.1016/j.bbamem.2010.02.012

88. Ramirez A, Crisafulli SG, Rizzuti M, et al. Investigation of New Morpholino Oligomers to Increase Survival Motor Neuron Protein Levels in Spinal Muscular Atrophy. *Int J Mol Sci*. 2018;19(1). doi:10.3390/ijms19010167

89. Moulton HM, Moulton JD. Morpholinos and their peptide conjugates: therapeutic promise and challenge for Duchenne muscular dystrophy. *Biochim Biophys Acta*. 2010;1798(12):2296-2303. doi:10.1016/j.bbamem.2010.02.012

90. Arumugam S, Garcera A, Soler RM, Tabares L. Smn-Deficiency Increases the Intrinsic Excitability of Motoneurons. *Front Cell Neurosci*. 2017;11:269. doi:10.3389/fncel.2017.00269

91. Quinlan KA, Reedich EJ, Arnold WD, et al. Hyperexcitability precedes motoneuron loss in the Smn2B/- mouse model of spinal muscular atrophy. *J Neurophysiol*. 2019;122(4):1297-1311. doi:10.1152/jn.00652.2018

92. Brunet A, Stuart-Lopez G, Burg T, Scekic-Zahirovic J, Rouaux C. Cortical Circuit Dysfunction as a Potential Driver of Amyotrophic Lateral Sclerosis. *Front Neurosci*. 2020;14:363. doi:10.3389/fnins.2020.00363

93. Lancaster MA, Knoblich JA. Generation of cerebral organoids from human pluripotent stem cells. *Nat Protoc*. 2014;9(10):2329-2340. doi:10.1038/nprot.2014.158

94. Mancinelli S, Lodato S. Decoding neuronal diversity in the developing cerebral cortex: from single cells to functional networks. *Curr Opin Neurobiol*. 2018;53:146-155. doi:10.1016/j.conb.2018.08.001

95. Tambalo M, Lodato S. Brain organoids: Human 3D models to investigate neuronal circuits assembly, function and dysfunction. *Brain Res*. 2020;1746:147028. doi:10.1016/j.brainres.2020.147028

96. Velasco S, Paulsen B, Arlotta P. 3D Brain Organoids: Studying Brain Development and Disease Outside the Embryo. *Annu Rev Neurosci*. 2020;43:375-389. doi:10.1146/annurev-neuro-070918-050154

97. Szebényi K, Wenger LMD, Sun Y, et al. Human ALS/FTD brain organoid slice cultures display distinct early astrocyte and targetable neuronal pathology. *Nat Neurosci*. 2021;24(11):1542-1554. doi:10.1038/s41593-021-00923-4

98. Ogura T, Sakaguchi H, Miyamoto S, Takahashi J. Three-dimensional induction of dorsal, intermediate and ventral spinal cord tissues from human pluripotent stem cells. *Development*. 2018;145(16):dev162214. doi:10.1242/dev.162214

99. Martins JMF, Fischer C, Urzi A, et al. Self-Organizing 3D Human Trunk Neuromuscular Organoids. *Cell Stem Cell*. 2020;26(2):172-186.e6. doi:10.1016/j.stem.2019.12.007

100. Ramos DM, d'Ydewalle C, Gabbeta V, et al. Age-dependent SMN expression in disease-relevant tissue and implications for SMA treatment. *J Clin Invest*. 2019;129(11):4817-4831. doi:10.1172/JCI124120

101. Barnat M, Capizzi M, Aparicio E, et al. Huntington's disease alters human neurodevelopment. *Science*. 2020;369(6505):787-793. doi:10.1126/science.aax3338

102. Galgoczi S, Ruzo A, Markopoulos C, et al. Huntingtin CAG expansion impairs germ layer patterning in synthetic human 2D gastruloids through polarity defects. *Development*. 2021;148(19):dev199513. doi:10.1242/dev.199513

103. Tharaneetharan A, Cole M, Norman B, et al. Functional Abnormalities of Cerebellum and Motor Cortex in Spinal Muscular Atrophy Mice. *Neuroscience*. 2020;452:78-97. doi:10.1016/j.neuroscience.2020.10.038

104. Simon CM, Janas AM, Lotti F, Tapia JC, Pellizzoni L, Mentis GZ. A Stem Cell Model of the Motor Circuit Uncouples Motor Neuron Death from Hyperexcitability Induced by SMN Deficiency. *Cell Rep*. 2016;16(5):1416-1430. doi:10.1016/j.celrep.2016.06.087

105. Wainger BJ, Kiskinis E, Mellin C, et al. Intrinsic membrane hyperexcitability of amyotrophic lateral sclerosis patient-derived motor neurons. *Cell Rep*. 2014;7(1):1-11. doi:10.1016/j.celrep.2014.03.019

106. Burg T, Bichara C, Scekic-Zahirovic J, et al. Absence of Subcerebral Projection Neurons Is Beneficial in a Mouse Model of Amyotrophic Lateral Sclerosis. *Ann Neurol*. 2020;88(4):688-702. doi:10.1002/ana.25833

107. Marques C, Burg T, Scekic-Zahirovic J, Fischer M, Rouaux C. Upper and Lower Motor Neuron Degenerations Are Somatotopically Related and Temporally Ordered in the Sod1

Mouse Model of Amyotrophic Lateral Sclerosis. *Brain Sci*. 2021;11(3):369. doi:10.3390/brainsci11030369

108. Negraes PD, Trujillo CA, Yu NK, et al. Altered network and rescue of human neurons derived from individuals with early-onset genetic epilepsy. *Mol Psychiatry*. 2021;26(11):7047-7068. doi:10.1038/s41380-021-01104-2

109. Prudencio M, Humphrey J, Pickles S, et al. Truncated stathmin-2 is a marker of TDP-43 pathology in frontotemporal dementia. *J Clin Invest*. 130(11):6080-6092. doi:10.1172/JCI139741

110. Finkel RS, Mercuri E, Darras BT, et al. Nusinersen versus Sham Control in Infantile-Onset Spinal Muscular Atrophy. *New England Journal of Medicine*. 2017;377(18):1723-1732. doi:10.1056/NEJMoa1702752

111. Duan D, Goemans N, Takeda S, Mercuri E, Aartsma-Rus A. Duchenne muscular dystrophy. *Nat Rev Dis Primers*. 2021;7(1):13. doi:10.1038/s41572-021-00248-3

112. Schindelin J, Arganda-Carreras I, Frise E, et al. Fiji: an open-source platform for biological-image analysis. *Nat Methods*. 2012;9(7):676-682. doi:10.1038/nmeth.2019

113. Livak KJ, Schmittgen TD. Analysis of relative gene expression data using real-time quantitative PCR and the 2(-Delta Delta C(T)) Method. *Methods*. 2001;25(4):402-408. doi:10.1006/meth.2001.1262

114. Tambalo M, Mitter R, Wilkinson DG. A single cell transcriptome atlas of the developing zebrafish hindbrain. *Development*. 2020;147(6). doi:10.1242/dev.184143

115. Rayon T, Maizels RJ, Barrington C, Briscoe J. Single cell transcriptome profiling of the human developing spinal cord reveals a conserved genetic programme with human specific features. *Development*. Published online July 16, 2021:dev.199711. doi:10.1242/dev.199711

116. Delile J, Rayon T, Melchionda M, Edwards A, Briscoe J, Sagner A. Single cell transcriptomics reveals spatial and temporal dynamics of gene expression in the developing mouse spinal cord. *Development*. 2019;146(12):dev173807. doi:10.1242/dev.173807

117. Reimand J, Isserlin R, Voisin V, et al. Pathway enrichment analysis and visualization of omics data using g:Profiler, GSEA, Cytoscape and EnrichmentMap. *Nat Protoc*. 2019;14(2):482-517. doi:10.1038/s41596-018-0103-9

118. Shannon P, Markiel A, Ozier O, et al. Cytoscape: a software environment for integrated models of biomolecular interaction networks. *Genome Res*. 2003;13(11):2498-2504. doi:10.1101/gr.1239303